Presynaptic LRP4 Promotes Synapse Number and Function of Excitatory CNS Neurons

Timothy J. Mosca[1,3*], David J. Luginbuhl[1], Irving E. Wang[2], and Liqun Luo[1]

[1] Howard Hughes Medical Institute and Department of Biology
Stanford University, Stanford, CA 94305 USA

[2] Department of Neurobiology
Stanford University, Stanford, CA 94305 USA

[3] Current Address: Department of Neuroscience
Thomas Jefferson University, Philadelphia, PA 19107

** Corresponding Author: Timothy J. Mosca (timothy.mosca@jefferson.edu)*

SUMMARY

Precise coordination of synaptic connections ensures proper information flow within circuits. The activity of presynaptic organizing molecules signaling to downstream pathways is essential for such coordination, though such entities remain incompletely known. We show that LRP4, a conserved transmembrane protein known for its postsynaptic roles, functions presynaptically as an organizing molecule. In the *Drosophila* brain, LRP4 preferentially localizes to excitatory neuron terminals at or near active zones. Loss of presynaptic LRP4 reduces excitatory (not inhibitory) synapse number, impairs active zone architecture, and abolishes olfactory attraction - the latter of which can be suppressed by reducing presynaptic $GABA_B$ receptors. LRP4 overexpression increases synapse number in excitatory and inhibitory neurons, suggesting an instructive role and a common downstream synapse addition pathway. Mechanistically, LRP4 functions via the conserved kinase SRPK79D to ensure normal synapse number and behavior. This highlights a presynaptic function for LRP4, enabling deeper understanding of how synapse organization is coordinated.

INTRODUCTION

Multiple levels of synaptic organization ensure accurate, controlled information flow through neuronal circuits. Neurons must first make an appropriate number of synaptic connections with their postsynaptic partners. Each of these synaptic connections must have appropriate strength that can be modified by plasticity and homeostasis as a result of experience and activity changes. Further, there must be an appropriate balance between excitatory and inhibitory synapses. Finally, recent work has shown that these connections also occupy precise locations with regards to the three-dimensional structure of the synaptic neuropil. Indeed, circuit models for diverse neuronal ensembles fail to recapitulate functional patterns unless these aspects are accounted for[1,2]. The misregulation of any one of these organizational parameters can result in neurodevelopmental disorders and intellectual disabilities like autism[3], epilepsy[4], and other synaptopathies[5]. Revealing the molecular mechanisms that ensure all of these facets are achieved is a critical step in understanding circuit assembly and function.

Synaptic organizers like Neurexins / Neuroligins, Teneurins, protein tyrosine phosphatases (PTPs), leucine rich repeat transmembrane proteins (LRRTMs), and Ephrin / Eph receptors, among others, ensure the proper number, distribution, and function of synaptic connections[6–11]. Loss-of-function mutations in these key synaptogenic molecules have deleterious structural, functional, and organizational consequences for synapses and circuits. At the vertebrate neuromuscular junction, one of these critical organizers is LRP4. There, it forms a receptor complex with MuSK in muscle fibers to promote clustering of acetylcholine receptors in response to motoneuron-derived agrin[12–14]. Muscle LRP4 can also function as a retrograde signal with an unknown motoneuron receptor to regulate presynaptic differentiation[15]. In these roles, the known functions from LRP4 are overwhelmingly postsynaptic. However, a number of lines of evidence suggest a broader role, beyond postsynaptic, for LRP4. First, motoneuron-derived LRP4 may regulate presynaptic differentiation, suggesting a role for neuronal LRP4[16]. Second, in the vertebrate central nervous system (CNS), agrin is not essential for synapse formation[17] though LRP4 can regulate synaptic plasticity, development, and

cognitive function[18,19], through functioning in astrocytes in some cases[20]. In this vein, the *Drosophila* genome contains an LRP4 homologue, but no clear agrin or MuSK homologues[21], so any role for LRP4 there must be agrin-independent.

Here, we show in the *Drosophila* CNS that LRP4 is a presynaptic protein that regulates the number, architecture, and function of synapses. LRP4 functions largely through the conserved, presynaptic SR-protein kinase, SRPK79D. LRP4 and SRPK79D interact genetically and epistatically, as SRPK79D overexpression can suppress *lrp4*-related phenotypes. Unexpectedly, this role for LRP4 occurs preferentially in excitatory neurons, as impairing *lrp4* in inhibitory neurons has no effect. As little is known about the presynaptic determinants (save neurotransmitter-related enzymes) of excitatory versus inhibitory synapses, this may suggest a new mode for distinguishing such synapses from the presynaptic side. Thus, LRP4 may represent a conserved synaptic organizer that functions presynaptically, cell autonomously, and independently of agrin to coordinate synapse number and function.

RESULTS

LRP4 is a synaptic protein expressed in excitatory neurons

We identified CG8909 as the fly LRP4 homologue (**Supplementary Fig. 1, 2a**), which is predicted to be a single-pass transmembrane protein whose domain organization resembles that of mammalian LRP4 (**Fig. 1a**). *Drosophila* LRP4 shares 38% identity with human LRP4 overall, 61% identity within the LDL-repeat containing extracellular portion, and 28% identity in the intracellular tail. Consistent with previous expression data from whole-brain microarrays[22], we determined that LRP4 was expressed throughout the adult brain using antibodies against the endogenous protein (**Fig. 1b-c**) or an *lrp4-GAL4* transgene that expresses GAL4 under the *lrp4* promoter and visualized with either Syt-HA (**Fig. 1d**) or an HA epitope-tagged LRP4 (**Supplementary Fig. 2c**). All methods revealed similar patterns of expression in the antennal lobe (**Fig. 1** and **Supplementary Fig. 2c-e**), optic lobe, and higher olfactory centers including the mushroom body and the lateral horn (**Fig. 1b, d**). Antibody specificity was validated by the complete loss of signal in a deletion (see below) of the *lrp4* coding region (**Fig. 1c**). We further investigated LRP4 in the antennal lobe, the first olfactory processing center in the *Drosophila* CNS, which has emerged as a model circuit for studying sensory processing[23] and whose synaptic organization was recently mapped at high resolution[24].

LRP4 was enriched in the synaptic neuropil of the antennal lobe (**Fig. 1b**). As this neuropil is made up of processes from multiple classes of olfactory neurons, all of which make presynaptic connections there, we used intersectional strategies with *lrp4-GAL4* to identify which neurons expressed *lrp4*. These approaches revealed *lrp4* expression in both olfactory receptor neurons (ORNs; **Supplementary Fig. 2d**) and projection neurons (PNs; **Supplementary Fig. 2e**). Because of the observed neuropil expression of LRP4 (**Fig. 1b-c**), we sought to examine the localization of LRP4 with regards to a known synaptic protein, the active zone scaffolding component Bruchpilot[25]. However, due to the density of CNS neuropil, colocalization analyses using light level microscopy have inherently low resolution. Therefore, we applied expansion microscopy[26] to the *Drosophila* CNS to improve the resolution of colocalization analysis. This technique uses isotropic expansion of immunolabeled tissue[27] while maintaining the spatial relationship between protein targets and allowing for enhanced resolution with confocal microscopy.

Using protein-retention expansion microscopy (proExM), we obtained reliable, ~4-fold isotropic expansion of *Drosophila* CNS tissue (**Supplementary Fig. 3**). To specifically examine the relationship between LRP4 and active zones only in ORNs, we expressed HA-tagged LRP4 and Brp-Short-mStraw using the SG18.1-GAL4 driver[28]. LRP4-HA expressed using *lrp4-GAL4* localizes to similar regions as LRP4 antibody staining (**Fig. 1b** and **Supplementary Fig. 2c**), suggesting the fidelity of this transgene. Within individual expanded glomeruli of proExM-treated brains, LRP4 and Brp localized to similar regions (**Fig. 1e**) and, when examined at high magnification, LRP4 localized either coincidentally with Brp (**Fig. 1f**, arrowhead) or to the space adjacent to active zones (**Fig. 1f**, arrow). This combination of active zone and periactive zone localization is similar to that of known synaptic organizers[29–31]. Thus, LRP4 is a synaptic protein that localizes to axon terminals.

Given widespread expression throughout the brain, we sought to identify the cell types that express LRP4. To accomplish this, we used *lrp4-GAL4* driven mCD8-GFP as this approach, in addition to labeling similar neuropil regions as the antibody, also highlighted the cell bodies of *lrp4*-positive cells. We co-stained brains for various cellular and neuronal-subtype markers and quantified the overlap between cells positive for *lrp4*-expression and expression of these various labels. Nearly all *lrp4*-positive cells observed (99.5%) expressed the neuronal marker ELAV[32] (**Fig. 1g**), indicating that these cells were neurons. Few (0.4%) expressed the glial marker Repo[33] (**Fig. 1h**). The majority of *lrp4*-positive cells (59.1%) also expressed choline acetyltransferase (ChAT; **Fig. 1i**), a marker for cholinergic excitatory neurons. We also observed partial overlap between *lrp4*-positive neurons and vGlut (22.4%; **Fig. 1j**), the vesicular transporter for glutamate; a subset of glutamatergic neurons are excitatory in the fly brain. Interestingly, there was little overlap (0.3%) between *lrp4* and GABA, the major inhibitory neurotransmitter in *Drosophila* (**Fig. 1k**). This suggests LRP4 is preferentially expressed at synaptic terminals of excitatory CNS neurons.

Perturbing presynaptic LRP4 changes ORN synapse number

As both the expression and localization of LRP4 were consistent with the protein serving a synaptic role, we sought to determine whether disrupting its function in excitatory neurons would affect synapse number. To image these connections, we expressed fluorescently tagged synaptic markers[24,34,35] and used previously established methods to estimate the number of active zones and postsynaptic receptor puncta[24] in olfactory neurons in antennal lobe glomeruli (**Fig. 2a**). These methods show stereotyped active zone numbers and densities in ORNs and can reveal the function of synaptic proteins in mediating these aspects[24]. Further, measurements from these methods are consistent with our own electron microscopy[24] as well as results from ultrastructural reconstructions of all synapses in individual glomeruli[36] demonstrating their utility. To perturb LRP4 function, we created a null mutation (*lrp4^{dalek}*) using the CRISPR-Cas9 system[37] that removed the entire coding region (**Supplementary Fig. 2a-b**). *lrp4^{dalek}* mutants were viable with a slightly reduced body size.

In ORN axon terminals projecting to the VA1v glomerulus in males (**Fig. 2b**), *lrp4^{dalek}* mutants (**Fig. 2c, h**) showed a 31% reduction in the number of puncta for Brp-Short, an active zone marker, compared to control adults (**Fig. 2b, h**). This phenotype was recapitulated when we expressed any of four independent transgenic RNAi

constructs against *lrp4* only in ORNs (**Fig. 2d, h**, and **Supplementary Fig. 4**), demonstrating that LRP4 functions presynaptically in regulating active zone number. These changes were independent of glomerular volume: *lrp4* loss-of-function had no effect on neurite volume (**Fig. 2h** and **Supplementary Fig. 4**). Though the intensity of Brp-Short puncta across some genotypes trended slightly downward, it did not reach statistical significance (data not shown). We also observed that *lrp4* disruption (using $lrp4^{dalek}$ mutants and presynaptic RNAi expression) caused a quantitatively similar reduction of active zone numbers in VA1v ORN axon terminals in females in this sexually dimorphic glomerulus **Supplementary Fig. 5**), and in ORN axon terminals projecting to the DA1, DL4, and DM6 glomeruli (**Supplementary Fig. 6**). This suggests that *lrp4* phenotypes are not specific to particular glomeruli. Beyond Brp-Short, we observed similar phenotypes with an independent presynaptic marker, DSyd-1[38], that is also punctate at ORN terminals[24] (**Supplementary Fig. 7**).

We further examined the consequences of *lrp4* disruption on the number of Dα7 acetylcholine receptor puncta in PN dendrites postsynaptic to the ORN axon terminals imaged above. Loss of *lrp4* decreased Dα7-EGFP puncta numbers by 29% compared to controls (**Fig. 2f-g, i**). This deficit was also independent of neurite volume (**Fig. 2i** and **Supplementary Fig. 4**), again demonstrating that *lrp4* perturbation phenotypes did not result from decreased neuronal projection size. Further, both the presynaptic active zone and postsynaptic acetylcholine receptor phenotypes were quantitatively similar. Thus, presynaptic LRP4 loss reduces synapse number as assayed both pre- and postsynaptically.

The above experiments demonstrated the necessity of presynaptic LRP4 in ensuring the proper number of synaptic connections. However, with known presynaptic organizers like Neurexin, overexpression results in added boutons[31] and active zones[39]. To test for LRP4 sufficiency in synapse addition, we overexpressed HA-tagged LRP4 presynaptically in otherwise wild-type ORNs. LRP4 overexpression increased the number of Brp-Short puncta by 30% (**Fig. 2e, h**, and **Supplementary Fig. 5**); this increase was also independent of neurite volume (**Fig. 2h** and **Supplementary Fig. 4, 5**) as the glomeruli remained the same size. Thus, there is a direct relationship between presynaptic LRP4 expression and synapse number in excitatory neurons: removing LRP4 reduces, while overexpressing LRP4 increases, synapse number.

Ultrastructural analysis reveals LRP4 regulates active zone number and structure

Though light level analyses accurately report fold-changes in synapse number[24,40], we sought to independently confirm and extend our analyses using electron microscopy. Using transmission electron microscopy (TEM) on the fly antennal lobe, we quantified synapse number in putative ORN terminals based on morphology[36,41] in both control (**Fig. 3a**) and $lrp4^{dalek}$ (**Fig. 3b**) adult brains. T-bar profiles were evident in both genotypes, but were reduced in number by 31% in mutant terminals (**Fig. 3c**), which exactly matched the reduction observed by Brp-Short puncta measurements (**Fig. 2h**). Terminal perimeter was slightly but significantly increased in $lrp4^{dalek}$ terminals (**Fig. 3d**), resulting in a 36% reduction in T-bar density when compared to control (**Fig. 3e**). These results are consistent with those observed via confocal microscopy, and demonstrate that LRP4 is necessary for the proper number of synapses in putative ORN terminals of the antennal lobe.

Brp-Short assays alone cannot distinguish between normal and impaired active zones. We therefore examined the ultrastructural morphology of individual active zones to determine if LRP4 had an additional role in the biogenesis of the T-bar itself. In both control (**Fig. 3f-h**) and *lrp4* (**Fig. 3i-k**) terminals, we observed single (**Fig. 3f, i**), double (**Fig. 3g, j**), and triple T-bars (**Fig. 3h, k**) suggesting that LRP4 is not absolutely required for T-bar formation and some elements of organization. However, whereas irregular T-bars in control animals were rare (<5% of total T-bars), the majority of T-bars in *lrp4* mutants displayed one or more defects (**Fig. 3l-q**), including immature T-bars that lacked tops (**Fig. 3l**), detached T-bars (**Fig. 3m**), misshapen T-bars of varying configurations and aggregations (**Fig. 3n-p**), and multiple T-bars beyond those observed in control animals (**Fig. 3q**). Thus, in addition to controlling the number of synapses, LRP4 is also required for individual active zones to assume normal morphology, attach to the membrane, and have proper spacing. Thus, LRP4 has multiple, critical roles in central synapse formation.

LRP4 is not required for inhibitory neuron synapse number

The preferential expression of *lrp4* in excitatory but not inhibitory neurons (**Fig. 1**) suggests that it promotes synapse addition specifically in excitatory neurons. To test this, we used Brp-Short to examine synapse number in GABAergic inhibitory neurons projecting to the antennal lobe using the *GAD1-GAL4* driver[42]. Though GAD1-positive neurons project throughout the antennal lobe[43], we restricted our analyses to the DA1 glomerulus, where we observed reductions in excitatory synapses (**Supplementary Fig. 6-7**) following LRP4 disruption. When LRP4 function was impaired using the *lrp4*^{dalek} mutant or RNAi in these neurons, synapse number was unaffected (**Fig. 4a-b, d**). Thus, the reduction of synapse number under LRP4 loss-of-function conditions appeared specific for excitatory neurons.

Interestingly, when LRP4 was overexpressed in inhibitory neurons, we observed a 35% increase in synapse number without an accompanying change in neurite volume, similar to what we observed for excitatory neurons (**Fig. 4c-d**). This suggests that, while inhibitory GABAergic neurons do not normally utilize LRP4 to regulate synapse number, they possess the downstream machinery necessary for LRP4 to function in adding synapses. Thus, when LRP4 is exogenously expressed in these cells, it can co-opt this machinery for synapse addition. As such, excitatory and inhibitory neurons likely use distinct cell surface synaptic organizers (LRP4 for excitatory neurons) that converge on common mechanisms for synapse addition.

Excitatory, but not inhibitory, olfactory projection neurons also require LRP4 to ensure proper synapse number

Though we initially restricted our analyses to the antennal lobe, we also observed *lrp4* expression throughout the brain, including two higher order olfactory neuropil: the mushroom body and the lateral horn (**Fig. 1b-d**). To determine whether LRP4 could also serve as a synaptic organizer in these brain regions, we examined the effects of *lrp4* perturbation on both excitatory and inhibitory synapses in the lateral horn (LH, **Fig. 5a**), a higher order olfactory center involved in innate olfactory behavior[44]. We used *Mz19-GAL4* to label projection neurons whose dendrites and cell bodies are restricted to the antennal lobe region, but whose axon terminals make excitatory synapses in the lateral horn[45]. To label inhibitory synapses, we used the *Mz699-GAL4* driver, which is expressed

in inhibitory projection neurons (iPNs) whose dendrites project to the antennal lobe and whose axons project to the lateral horn[46,47]. *Mz699-GAL4* also labels a small subset of third-order neurons that project dendrites largely void of presynaptic terminals to the ventral lateral horn[46]. Thus, we consider synaptic signal labeled by *Mz699-GAL4* as being contributed mostly by iPNs.

In *lrp4* mutants, the number of excitatory lateral horn synapses was reduced by 40%, consistent with a role for LRP4 in synapse formation (**Fig. 5b-c, f**). PN perturbation of *lrp4* using RNAi reduced synapse number similarly to the loss-of-function allele, demonstrating a presynaptic role for *lrp4* in these neurons (**Fig. 5f** and **Supplementary Fig. 8**). These changes were independent of neurite volume, which remained unaffected (**Fig. 5f**). Perturbation of *lrp4* in *Mz699*-positive iPNs, however, had no effect on the number of synapses (**Fig. 5d-e, g**, and **Supplementary Fig. 8**) despite a slight reduction in neurite volume in *lrp4^{dalek}* mutants (**Fig. 5g**). Despite a lack of a loss-of-function phenotype, we observed an increase in synapse number when we overexpressed LRP4-HA in *Mz699*-positive neurons (**Fig. 5g** and **Supplementary Fig. 8**). Thus, the results of *lrp4* perturbation on excitatory and inhibitory synapses in the lateral horn resembled those of the antennal lobe, suggesting a general role for LRP4 in promoting excitatory synapse number.

LRP4 is required for normal olfactory attraction behavior

Given the role for LRP4 in the specific regulation of excitatory synapse number, we sought to determine whether the consequences of LRP4 disruption were accompanied by functional changes in behavior. We examined fly attraction to the odorant in apple cider vinegar using a modified olfactory trap assay[48,49] (**Fig. 6a**), an ethologically relevant assay that requires flight and/or climbing to follow odorant information within a larger arena[50]. As presynaptic LRP4 regulates ORN synapse number, we used RNAi against *lrp4* expressed selectively in all ORNs using *pebbled-GAL4* to assess olfactory attraction. Control flies bearing a single copy of *pebbled-GAL4* or one of four different *lrp4* RNAi transgenes alone exhibited a strong preference for apple cider vinegar (**Fig. 6b**). Flies bearing both transgenes (and thus, reduced *lrp4* expression) exhibited a near complete abrogation of attractive behavior and were no longer able to distinguish the attractive apple cider vinegar from a water control (**Fig. 6b**). Movement, wall climbing, and flight were still observed in these flies (data not shown), suggesting that this was not due to widespread defects in motion, consistent with our selective perturbation of LRP4 function in ORNs. Thus, presynaptic LRP4 in ORNs is necessary for normal olfactory attraction behavior.

A complete loss of olfactory attraction was unexpected for a manipulation that reduced synapse number by ~30%. One potential explanation is that, while the remaining 70% of synapses were detected by the Brp-Short assay, they were functionally impaired. This would be consistent with the myriad of morphology defects observed in *lrp4* mutant T-bars via TEM (**Fig. 3i-q**). In *Drosophila*, olfactory information flow is regulated by presynaptic inhibition by local GABAergic interneurons onto excitatory ORNs via the $GABA_A$ and $GABA_BR2$ receptors[51,52]. If the remaining synapses were indeed weakened by the loss of LRP4, reducing inhibition onto those ORNs might suppress the behavioral phenotype. To test this hypothesis, we inhibited the $GABA_BR2$ receptor in ORNs using RNAi, which by itself did not affect the olfactory attraction behavior (**Fig. 6b**).

Simultaneous knockdown of *GABA$_B$R2* and *lrp4*, however, markedly suppressed the behavioral phenotype associated with *lrp4* knockdown alone (**Fig. 6b**). This manipulation did not suppress the morphological phenotype, however, as the reduction in Brp-Short puncta was still apparent (1297 ± 25.62 puncta, *n* = 39 antennal lobes for *Or47b-GAL4 > UAS-lrp4^{IR2} + UAS-mCD8-GFP* vs. 1191 ± 48.91 puncta, *n* = 12 antennal lobes for *Or47b-GAL4 > UAS-lrp4^{IR2} + UAS-GABABR2^{IR}*, *p* > 0.2). These results suggest that olfactory attraction behavior requires a proper level of net excitatory drive in the antennal lobe circuit and that defects caused by weakened excitatory synapses can be compensated for by reducing inhibition.

SRPK79D interacts with, and requires, LRP4 for ORN terminal localization

To understand how LRP4 could regulate excitatory synapse number and olfactory behavior, we investigated the mechanism by which it functions. In examining *lrp4^{dalek}* mutant larvae and larvae where *lrp4* was specifically knocked down in all neurons using RNAi, we observed impaired localization of active zone material (**Fig. 7a-c**). Under normal circumstances, the active zone marker Bruchpilot[25] and the synaptic vesicle marker Synaptotagmin I[53] were barely detectable in larval transverse nerves (**Fig. 7a**), due to their proper trafficking to or maintenance at synaptic sites. However, in *lrp4^{dalek}* mutants, Bruchpilot improperly accumulated in the transverse nerves (**Fig. 7b**). This kind of accumulation is rarely observed in wild type, but is also most notably associated with loss of SRPK79D (**Fig. 7c**), a conserved serine-arginine protein kinase that localizes to NMJ terminals and negatively regulates premature active zone assembly before Bruchpilot reaches the fly NMJ[54,55]. In both *lrp4* and *srpk79D* mutants, Brp accumulation was not accompanied by focal accumulations of Synaptotagmin I, indicating that axonal trafficking is not generally impaired (**Fig. 7a-c**)[54–56]. Because of the similarity in the transverse nerve phenotypes and the role of SRPK79D at peripheral synapses, we hypothesized that LRP4 and SRPK79D could operate together in the CNS to regulate synapse number.

As SRPK79D antibodies are not available, we utilized Venus-tagged SRPK79D transgenes to examine CNS localization. When expressed only in VA1v ORNs, venus-SRPK79D localized to axon terminals and overlapped with Brp-Short, demonstrating localization with and adjacent to CNS active zones (**Fig. 7d**). This was reminiscent of LRP4-HA localization in ORNs (**Fig. 1f**) so we turned to proExM to more precisely assess the spatial relationship between SRPK79D and LRP4. In the ORNs of expanded individual glomeruli, LRP4-HA and venus-SRPK79D exhibited coincident and adjacent localization (**Fig. 7e**). However, SRPK79D was expressed more broadly throughout ORNs, suggesting that only a subset of SRPK79D colocalizes with LRP4. This may indicate both LRP4-dependent and –independent roles for SRPK79D. We also examined this synaptic localization in *lrp4^{dalek}* mutants: loss of *lrp4* reduced synaptic SRPK79D levels by ~50% (**Fig. 7f-h**). This reduction was specific for SRPK79D, as the staining for other markers, like the general neuropil label N-Cadherin, was unaffected (**Fig. 7f-h**). These results demonstrate that LRP4 is necessary for the proper localization and / or expression of SRPK79D and suggest that SRPK79D might act downstream of LRP4 to regulate synapse number.

Due to their spatial proximity, we next employed proximity ligation assays (PLA) to determine whether LRP4 and SRPK79D are spatially close enough to interact. PLA uses oligonucleotides conjugated to secondary antibodies[57,58]: if the epitopes are sufficiently

close (30–40 nm), the oligonucleotides can be ligated together and detected using a fluorescent probe. The result can be observed using confocal microscopy and preserve, to a high degree, the spatial localization of the proteins involved. PLA has been used to examine protein-protein interactions at the NMJ[59] but not, to our knowledge, in the CNS. To examine this, we co-expressed venus-SRPK79D and LRP4-HA in all ORNs using *pebbled-GAL4*[60], stained both targets with oligonucleotide-conjugated secondary antibodies and performed PLA assays (**Fig. 7i-j** and **Supplementary Fig. 9**). As expected, both proteins localize to the axon terminals of ORNs. When either is expressed singularly (**Supplementary Fig. 9a-b**) or the probes are not added (**Fig. 7i**), no PLA signal is observed. However, in the presence of both transgenes and the appropriate probes (**Fig. 7j** and **Supplementary Fig. 9c-d**), we detected positive signal indicating that the proteins were close enough to interact. The PLA signal represented a subset of LRP4 or SRPK79D staining patterns, suggesting that there are roles independent of the other for each protein. Taken together, this data suggests that LRP4 interacts with SRPK79D to maintain its localization at the synapse.

SRPK79D overexpression suppresses LRP4 phenotypes

The interaction with, and reliance on LRP4 for synaptic SRPK79D localization suggested that the two function together. If so, we would expect that the two would display phenotypic similarity and interact in the same genetic pathway. We observed phenotypic similarity in larval nerves (**Fig. 7a-c**), but we further sought to study this at CNS synapses. To test the interactions between LRP4 and SRPK79D with respect to effects of synapse number, we conducted loss-of-function, genetic interaction, and genetic epistasis experiments between genetic perturbations of both. First, reducing *srpk79D* function presynaptically using an established RNAi[54] expressed in VA1V ORNs resulted in a 15% reduction in the number of Brp-Short puncta compared to control (**Fig. 8a-b, e**). Thus, SRPK79D is required for normal CNS synapse number. We further sought to understand if LRP4 and SRPK79D interacted genetically. To examine this, we performed a transheterozygote genetic interaction assay. When single copies of either *lrp4* or *srpk79D* were removed, there was no evident phenotype (**Supplementary Fig. 10b-c, e**). However, when one copy of each was concurrently removed, we observed a significant reduction in Brp-Short puncta (**Supplementary Fig. 10d-e**). This suggests that the two function in the same genetic pathway and may work together to ensure proper synapse number. Given the reduction in synaptic SRPK79D present in *lrp4* mutants, we examined whether these reduced SRPK79D levels are the root cause of its synapse reduction. We overexpressed SRPK79D in presynaptic ORNs either in control or $lrp4^{dalek}$ mutant backgrounds. Presynaptic overexpression of SRPK79D in VA1v ORNs partially suppressed the synaptic phenotype associated with the $lrp4^{dalek}$ mutation, resulting in 92% of the normal number of synapses (**Fig. 8a, c-e**), whereas overexpression of SRPK79D in a wild-type background had no effect (**Fig. 8e**). Finally, we sought to determine whether *srpk79D* was required for the increase in Brp-Short puncta associated with LRP4 overexpression (**Fig. 2h**). When LRP4 was overexpressed concurrently with *srpk79D* RNAi, the phenotype resembled that of *srpk79D* RNAi alone (**Fig. 8e**). This suggests that LRP4 requires SRPK79D to mediate its overexpression phenotype, likely by functioning through SRPK79D to increase the number of synapses. Combined, these

indicate that LRP4 and SRPK79D closely interact presynaptically in the same genetic pathway to ensure the proper number of excitatory synapses.

In light of the synapse number defects, we also examined the functional consequences of *srpk79D* perturbation on olfactory behavior. Flies expressing *srpk79D* RNAi in all ORNs demonstrated a nearly complete abrogation of attraction behavior (**Fig. 8f**) that was indistinguishable from the *lrp4* RNAi phenotype. In light of the suppression of the synapse number phenotype, we also examined whether SRPK79D overexpression could suppress the *lrp4* loss-of-function behavioral phenotype. Control flies bearing the pan-ORN *pebbled-GAL4* or the SRPK79D overexpression transgene alone exhibited strong attraction towards apple cider vinegar (**Fig. 8f**). Further, SRPK79D overexpression in all ORNs did not affect this robust attraction. Driving both SRPK79D overexpression and *lrp4* RNAi in all ORNs, however, resulted in a partial suppression of the behavioral phenotype associated with *lrp4* RNAi (**Fig. 8f**). As the synaptic level of SRPK79D is positively regulated by LRP4 and SRPK79D overexpression suppresses the morphological and functional phenotypes associated with *lrp4* loss-of-function, SRPK79D is likely a key downstream effector of LRP4 in regulating synapse number and thus, normal olfactory attraction behavior.

DISCUSSION

Understanding how synaptic organizers regulate the number and function of synapses in the CNS is a central goal of molecular neurobiology. This study identifies LRP4 as a synaptic protein whose expression is preferential for excitatory neurons in the *Drosophila* CNS (**Fig. 1**). Though well-known as the postsynaptic agrin receptor at the mouse NMJ[13,61], here we describe an agrin-independent, presynaptic role for LRP4. In the *Drosophila* CNS, LRP4 functions presynaptically to regulate the number of active zones in presynaptic ORNs (**Fig. 2-3**) and acetylcholine receptor clusters in the PNs postsynaptic to those ORNs (**Fig. 2**). Moreover, LRP4 also controls the morphology of individual active zones: *lrp4* mutant T-bars exhibit striking defects in patterning and biogenesis (**Fig. 3**). These defects are specific for excitatory neurons, as inhibitory neuron synapses in the antennal lobe remain unaffected (**Fig. 4**). Overexpression of LRP4, however, can increase synapse number cell autonomously in both excitatory and inhibitory neurons (**Fig. 2-4**), suggesting that both share common mechanisms for synapse addition. The role for LRP4 further extends to higher order olfactory neuropil in the lateral horn (**Fig. 5**), suggesting that it may serve a general role in synaptic organization. Underscoring the functional importance of LRP4, its perturbation in excitatory ORNs abrogated olfactory attraction behavior (**Fig. 6**). The suppression of the behavioral phenotype by reducing presynaptic inhibition onto ORNs further suggests that a proper level of excitatory drive is important for functional circuit output. To mediate both morphological and behavioral effects, LRP4 likely functions through SRPK79D, a conserved SR-protein kinase whose loss-of-function phenotypes resemble those of *lrp4* (**Fig. 7-8**), whose synaptic localization depends on LRP4 (**Fig. 7**), who interacts genetically with and is physically in proximity to LRP4 (**Fig. 7-8**) and whose overexpression suppresses the phenotypes associated with loss of *lrp4* (**Fig. 8**).

LRP4 as a synaptic regulator that distinguishes excitatory from inhibitory presynaptic terminals

Coordination of excitation and inhibition is critical to proper circuit function. Imbalances in excitation and inhibition lead to epileptic states[62] and social dysfunction[63], and may also underlie many autism spectrum disorders[3,64]. The mechanisms that maintain this balance are incompletely understood, though likely involve multiple aspects including the number of each type of neuron, their firing rates, release probabilities, synaptic strength, and neurotransmitter receptor sensitivities. Such regulation likely requires distinguishing excitatory from inhibitory neurons at both pre- and postsynaptic levels. Excitatory and inhibitory synapses are identified postsynaptically by distinct neurotransmitter receptor, scaffolding protein, and adhesion molecule repertoires[39,65,66]. Postsynaptic factors like Neuroligin 2[67], Gephyrin[68], and Slitrk3[69] organize inhibitory GABAergic synapses while LRRTMs organize excitatory synapses[70–72]. Thus, postsynaptic regulation can occur by differential modulation of these factors. Little is known, however, about the presynaptic identifiers of excitatory versus inhibitory neurons. Recent work identified Punctin / MADD-4 as a determinant of excitatory versus inhibitory neuromuscular synapses in *C. elegans*, though as a secreted factor that functions via postsynaptic interaction[73–75]. Further, Glypican4 can localize to excitatory presynaptic terminals and interact with LRRTM4[71] but its synaptogenic activity is also provided by astrocytes[76] and thus is not neuronal specific. Proteomic comparisons[77,78] suggest few differences beyond those pertaining to neurotransmitter synthesis enzymes and transporters. But these components may not be sufficient to distinguish presynaptic excitatory from inhibitory neurons. In the *Drosophila* olfactory system, for example, glutamate can be inhibitory when its postsynaptic partners express glutamate-gated chloride channels[79]. This suggests that pre- and postsynaptic regulators may exist to distinguish excitatory and inhibitory synapses, though it is unclear what those presynaptic regulators might be.

Our data suggests that LRP4 is a candidate presynaptic organizer specific for excitatory connections. Consistently, LRP4 expression overlaps considerably with cholinergic, but not GABAergic, neurons (**Fig. 1**). For glutamatergic olfactory neurons, there is only partial overlap with LRP4 (**Fig. 1**), consistent with these neurons serving either excitatory or inhibitory roles. LRP4, however, does not only serve an identifying role at excitatory synapses, but also a functional one. Loss of *lrp4* results in fewer excitatory synapses but has no effect on inhibitory synapses. However, both excitatory and inhibitory neurons show increased synapse number with *lrp4* overexpression (**Fig. 2, 4-5**). This shared competency suggests that both neurons contain machinery that can be engaged downstream of LRP4 (or the cell surface) to add synapses. Thus, proteins like LRP4 may represent identifiers of excitatory or inhibitory terminals that function by engaging common mechanisms to add synapses.

.

LRP4 function across evolution

At the mouse NMJ, LRP4 is the well-established postsynaptic receptor for motoneuron-derived Agrin[13,61,80] and regulates synapse formation[12] and maintenance[14]. However, additional roles for LRP4 exist for at the level of the presynaptic motoneuron. A retrograde signal composed of LRP4 from the postsynaptic muscle interacts with an unknown receptor in the motoneuron[15] to regulate presynaptic differentiation. Thus, at the mouse

NMJ, postsynaptic LRP4 has both cell-autonomous and non-cell autonomous roles. In addition, presynaptic LRP4 has been implicated to regulate acetylcholine receptor clustering via MMP-mediated proteolytic cleavage[16].

In the mouse CNS, LRP4 regulates synaptic physiology[18,19], learning and memory, fear conditioning, and CA1 spine density[18]. Though CNS LRP4 most commonly associates with postsynaptic densities[81], it also fractionates with synaptophysin-positive membranes[18]. Indeed, the observed CNS phenotypes have not been localized to a particular pool of LRP4. Our identification of *Drosophila* LRP4 as a key player in CNS synaptogenesis, however, posits a cell-autonomous presynaptic role. While we cannot rule out an additional postsynaptic role, our work is the first to demonstrate clear cell-autonomous presynaptic functions for LRP4. Moreover, as the *Drosophila* genome lacks clear Agrin and MuSK homologs, this suggests a synaptic function of LRP4 that evolutionarily precedes Agrin and MuSK recruitment to vertebrate NMJ synaptogenesis.

It remains open whether this presynaptic function is conserved in the mammalian CNS and, if so, what signal LRP4 receives. In *Drosophila*, the signal cannot be Agrin and in the mammalian CNS, Agrin is not essential for CNS synapse formation[17]. Thus, the Agrin-independence of CNS LRP4 may be conserved across systems. Moreover, our finding that LRP4 promotes excitatory, but not inhibitory, synapse formation and function is consistent with reduced excitatory but normal inhibitory input in hippocampal CA1 neurons of *lrp4* mutant mice[18]. Moreover, we find that LRP4 in the *Drosophila* CNS functions through the SR-protein kinase SRPK79D. Impaired *srpk79D* function reduces synapse number and overexpression can suppress the functional and morphological defects associated with *lrp4* loss (**Fig. 7-8**). This kinase is evolutionarily conserved[54] and the three mammalian homologues[82] are widely expressed in the mouse brain[83], including in the hippocampus. From yeast to human, SRPKs regulate spliceosome assembly and gene expression[82] but have not been studied in mammalian synapse formation. It will be interesting to test if these kinases also function in the mammalian CNS. Combined, however, these commonalities suggest a basic conservation between invertebrate and vertebrate systems for future study.

Connecting LRP4 and human disease

Recent work implicated LRP4 in both amyotrophic lateral sclerosis (ALS) and myasthenia gravis (MG), two debilitating motor disorders with a worldwide prevalence of ~1/5000. Distinct ALS and MG populations are seropositive for LRP4 autoantibodies[84,85] and double seronegative for Agrin or MuSK, suggesting that seropositivity is not a byproduct of generalized NMJ breakdown. Further, injection of LRP4 function-blocking antibodies into mice recapitulates MG[86]. Beyond peripheral symptoms, cognitive impairment (besides that as frontotemporal dementia) also occurs in a subset of ALS patients[87]. Thus, understanding the roles of LRP4 in the peripheral and central nervous systems has marked clinical significance. Our identification of an evolutionarily conserved kinase, SRPK79D, as a downstream target of LRP4 signaling may offer a window into those roles. As SRPK79D overexpression suppresses the behavioral and the synaptic phenotypes of *lrp4* loss (**Fig. 8**), if it functions similarly in the mammalian CNS, SRPKs could be a target for therapeutics. Further investigation of how LRP4 functions in the CNS will provide new insight not only into the cognitive aspects of these debilitating motor disorders, but also into the fundamental aspects of excitatory synapse formation.

EXPERIMENTAL PROCEDURES

Generation of lrp4 CRISPR mutants.

The *lrp4* mutation was designed following published methods[37]. Two *lrp4*-specific chimeric RNAs (chiRNA) were cloned into the pU6-BbsI-chiRNA vector as follows - A1, corresponding to an optimal PAM site 2 bp 5' of the start ATG (using primers: 5' CTTCGGCGAGTTTGTGTACATGTC 3' and 5' AAACGACATGTACACAAACTCGCC 3' with a phosphate at the 5' end) and A2, corresponding to an optimal PAM site 34 bp 3' of the TAG stop codon (using primers 5' CTTCGAATCGGTAAATGGTTTCAG 3' and 5' AAACCTGAAACCATTTACCGATTC 3'). Both the A1 and A2 chiRNA plasmids (250 ng / µL) and a pHsp70-Cas9 plasmid (500 ng / µL) were injected into MB03015 embryos (stock BL23835) to produce *lrp4* deletions. MB03015 flies bear a Minos-based Mi{ET1} insertion[88] between exons 5 and 6 of the *lrp4* open reading frame; adults with the insertion are marked by expression of a GFP reporter in the eye. Successful events were screened for by the loss of GFP: as the PAM sites were distant from and flanking the insertion, loss of fluorescence likely indicated removal of the intervening sequences (the *lrp4* coding region). Five such lines (representing identical events) were recovered and homozygous viable stocks established: the allele was named *dalek* due to the "extermination" of the *lrp4* gene, and in homage to the classic villains of 'Doctor Who'. Loss of *lrp4* was assessed using genomic DNA prepared from control and $lrp4^{dalek}$ adults using the QIAgen DNeasy Blood and Tissue Kit (QIAgen, Valencia, CA). Genomic PCR bands corresponding to exon 2 (534 bp using primers 5' TGTATTCCACGAACCTGGGTATG 3' and 5' CAAAATGCAGCGCCCATTGTT 3') and the exon 7-8 junction (615 bp using primers 5' AGTCTTGATGGTAGCAATAGGCAT 3' and 5' CTCTGGTAGATTTTGACACTG 3') revealed the absence of both regions in $lrp4^{dalek}$. The $lrp4^{dalek}$ deletion was further confirmed by the presence of a 315 bp 'Flank' band (with some background bands present only with the $lrp4^{dalek}$ deletion) representing the connection of sequences from the 5' and 3' UTRs (amplified by primers 5' AACAGAATCGGAACAGCAGTT 3' and 5' GAGCTTTAACAGGACACGTTT 3') not present in control samples (see Fig. S1b). Finally, antibody staining (see Supplementary Experimental Procedures) revealed the elimination of LRP4 signal in the $lrp4^{dalek}$ allele, suggesting the creation of a null allele.

Cloning of LRP4 cDNA and Transgene Construction.

An adult *Drosophila* cDNA library was made according to manufacturer's protocol using the GeneRacer Kit (Invitrogen, Carlsbad CA). From the library, the *lrp4* cDNA was amplified using the forward primer 5' CACCATGTATTTGACAGCCTTT 3' and the reverse primer 5' TGTGATAGTCGAGAGCGT 3' (without the endogenous Stop codon) and cloned directly into the pENTR vector using the pENTR/D-TOPO Cloning Kit (Invitrogen, Carlsbad, CA). Complete cDNA clones were verified by sequencing. UAS-LRP4-HA was made by recombining pENTR-LRP4 with pUAST-attB-Gateway-3xFLAG-3xHA[29] via LR clonase. The resultant pUAST-attB-LRP4-3xHA-3xFLAG was transformed into the ΦC31 landing site 86Fb on the 3rd chromosome using standard methods.

Production of LRP4 antibodies.

Custom antibodies were made by Pierce Custom Services (ThermoFisher, Rockford, IL) against the C-NKRNSRGSSRSVLTFSNPN peptide corresponding to residues 1921-

1939 of the intracellular side of LRP4. Rat antisera were Ig-purified and then used at a dilution of 1:200 on adult brains. The specificity of the antibody was verified by the absence of signal in the *lrp4*^{dalek} mutant.

Alignment of LRP4 homologues.
The *Drosophila melanogaster* (CG8909; accession AAF48538.1), *Mus musculus* (accession NP_766256.3), and *Homo sapiens* (accession NP_002325.2) LRP4 sequences were obtained from NCBI. CLUSTALW alignment was performed using PSI/T-Coffee for transmembrane proteins (http://tcoffee.crg.cat/apps/tcoffee/do:tmcoffee) and expressed graphically using ESPript3.0 (http://espript.ibcp.fr/ESPript/ESPript/).

***Drosophila* stocks and transgenic strains.**
All controls, stocks, and crosses were raised at 25°C. Mutants and transgenes were maintained over balancer chromosomes to enable selection in adult or larval stages. The GMR90B08-GAL4[89] line was used to examine *lrp4* expression (referred to as *lrp4*-GAL4). Four UAS-RNAi lines against differing regions of *lrp4* were also identified: *UAS-lrp4-RNAi 1* (v29900, Vienna Drosophila Resource Center), *UAS-lrp4-RNAi 2* (v108629, Vienna Drosophila Resource Center), *UAS-lrp4-RNAi 3* (JF01570, Harvard TRiP Collection), *UAS-lrp4-RNAi 4* (JF01632, Harvard TRiP Collection). The following GAL4 lines enabled tissue-specific expression: *Or47b-GAL4* (VA1v ORNs) [90], *Or67d-GAL4* (DA1 ORNs)[91], *Or88a-GAL4* (VA1d ORNs)[90], *AM29-GAL4* (DL4 and DM6 ORNs) [92], *Mz19-GAL4* (DA1, VA1d, DC3 PNs)[93], *Mz699-GAL4* (inhibitory projection neurons that project to the lateral horn)[46,47], *GAD1-GAL4* (GABAergic inhibitory neurons) [42], *pebbled-GAL4* (all ORNs)[60]. The following UAS transgenic lines were used as either reporters or to alter gene function: UAS-Syt-HA[94], *UAS-Brp-Short-mStraw*[34], *UAS-DSyd1-GFP* [95], *UAS-Dα7-GFP*[35], *UAS-mCD8-GFP*[96], *UAS-3xHA-mtdT*[48], *UAS-FRT-Stop-FRT-mCD8-GFP*[97], *UAS-Dcr2*[98], *UAS-GABA$_B$R2-RNAi*[51], *UAS-srpk79D-RNAi*[54], *UAS-venus-SRPK79D-#28*[54], *UAS-venus-SRPK79D-#1A*[54]. Intersectional analyses were done using the *eyFLP$^{3.5}$* construct[99] which expresses FLP in ORNs, but not PNs and *GH146-FLP*[97], which expresses in 2/3 of all olfactory PNs but not ORNs. The *srpk79D^{atc}* allele[54] was used to remove *srpk79D* function.

Immunocytochemistry.
Adult brains were dissected at 10 days post eclosion as previously described[24,100]. Third instar larvae were dissected as previously described[101]. The following primary antibodies were used: mouse antibody to Bruchpilot (mAbnc82, 1:40)[102], rabbit antibody to Synaptotagmin I (1:4000)[103], rat antibody to N-Cadherin (mAbDN-EX #8, 1:40)[104], rat antibody to HA (3F10, Roche, 1:100), mouse antibody to choline acetyltransferase (ChAT, mAbChAT4B1, 1:100)[105], mouse antibody to ELAV (mAb9F8A9, 1:100)[106], rabbit antibody to GABA (Sigma, 1:200), mouse antibody to Repo (mAb8D12, 1:100)[107], rabbit antibody to vGlut (1:500)[108], rabbit antibody to dsRed (Clontech, 1:500), chicken antibody to GFP (Aves Labs, 1:1000), Cy5-conjugated goat antibody to HRP (1:100, Jackson ImmunoResearch). Alexa488-, Alexa568-, and Alexa647-conjugated secondary antibodies were used at 1:250 (Invitrogen). CF633-conjugated secondary antibodies were used at 1:250 (Biotium). FITC-conjugated secondary antibodies were used at 1:200 (Jackson ImmunoResearch).

Proximity ligation assay.
Brains were processed as described and stained using rabbit anti-GFP antibodies at 1:500 (Invitrogen, Carlsbad, CA) with FITC-conjugated secondary antibodies and mouse anti-HA antibodies at 1:250 (Invitrogen, Carlsbad, CA) with Alexa647-conjugated secondary antibodies, leaving the red channel open. For PLA, we used the DuoLink Mouse Rabbit *In Situ* PLA kit (Sigma-Aldrich, St. Louis, MO). Following the last wash after secondary antibody incubation, the brains were incubated in the anti-mouse and / or anti-rabbit PLA probes at a 1:5 dilution for 2 hours at 37°C. Brains were then washed thrice for 10' each with Wash Buffer A, and incubated in Ligation solution (1:40 ligase in ligation buffer) for 1 hour at 37°C. Brains were washed in Wash buffer A for three times at 10' each and then incubated in Amplification solution (1:80 dilution of polymerase in Amplification buffer) for 2 hours at 37°C. Finally, brains were washed three times for 10' each in Wash Buffer B, and incubated in SlowFade overnight before mounting. Controls without Probes went through the identical process as those with probes, but with water substituted for the probes themselves in the first PLA step. Brains were imaged as described via confocal microscopy.

Imaging, synaptic quantification and image processing.
All images were obtained using a Zeiss LSM510 Meta laser-scanning confocal microscope (Carl Zeiss, Oberkochen, Germany) using either a 40X 1.4 NA PlanApo or a 63X 1.4 NA PlanApo lens. Images of synaptic puncta (Brp-Short-mStraw or Dα7-GFP) and neurite membrane (mCD8-GFP, 3xHA-mTDT) were imaged, processed and quantified as previously described[24] with the following adjustments: images of synaptic puncta in the lateral horn (Mz19-GAL4, Fig. S5; Mz699-GAL4, Fig. S7) were imaged at 63X, with an optical zoom of 2. Mz19 and Mz699 images were processed with a spot size of 0.6 µm and neurite volume calculated with a smoothing of 0.2 µm and a local contrast of 0.5 µm.

Images were processed and figures prepared using Adobe Photoshop CS4 and Adobe Illustrator CS4 (Adobe Systems, San Jose, CA). For antibody staining comparisons between genotypes, samples were imaged and processed under identical conditions. Fluorescence intensity was measured with ImageJ (NIH, Bethesda, MD).

Electron microscopy.
Transmission electron microscopy was performed on 10 day old adult control and *Irp4*^{dalek} male brains as previously described[24]. Putative ORN terminals were identified based on morphology[36,41] and quantified as described[24]. Terminal perimeter was measured using ImageJ (NIH, Bethesda, MD) and used to calculate T-bar density. All quantification was done with the user blind to the genotype.

Expansion microscopy.
Protein retention expansion microscopy[27] was modified for use with *Drosophila* brain tissue. Fixed and antibody-labeled brains were treated with 100 µg / mL acryloyl-X, SE (ThermoFisher) overnight at room temperature and then embedded in polyelectrolyte gel for two hours at 37°C. Slices containing brains were excised from solidified polyelectrolyte gel and immersed in digestion buffer with 200 µg / mL Proteinase K (Ambion) overnight

at room temperature. Slices achieved maximum expansion after five washes with deionized water. Fully expanded gel slices were anchored to the bottom of a petri dish with 2% low melting point agarose. Confocal microscopy images were obtained with a 25x water immersion objective (Leica SP8).

Statistical analysis.
Statistical analysis was completed using Prism 6.07 (GraphPad Software, Inc., La Jolla, CA). For representative datasets, the experimenter was blind to genotype during quantification and data analysis. Significance between two samples was determined using student's t-test. Significance amongst multiple samples was determined using one-way ANOVA with a Tukey's post-test to correct for multiple comparisons. Significance between two samples (for EM) was determined using a two-tailed student's t-test.

Behavioral analyses.
Olfactory trap assays were constructed as described[48]. Flies were raised in a 12/12 light/dark incubator. For each cohort, 25 flies of the appropriate genotype were starved overnight in a 1% agar vial in complete darkness. They were anesthetized briefly on ice and transferred to the olfactory trap, which contained an experimental vial of apple cider vinegar (ACV: Safeway, Palo Alto, CA) and a control vial of water. Flies were then left in the trap for 16 hours in complete darkness before being quantified. Preference index was calculated as ($Flies_{ACV}$ – $Flies_{Water}$) / $Flies_{Total}$. For all cases, $n \geq 6$ cohorts of flies per genotype.

Genotypes.
Fig. 1: (b) *+; +; +;* +. (c) *lrp4^{dalek} / Y; +; +;* +. (d) w, UAS-Syt-HA / Y*; +; lrp4-GAL4 / +;* +. (e-f) w, *pebbled-GAL4 / Y; +; UAS-LRP4-HA / +;* +. (g-k) *+; UAS-mCD8-GFP / +; lrp4-GAL4 / +;* +. **Fig. 2**: (b) *UAS-Dcr2 / Y; UAS-Brp-Short-mStraw, UAS-mCD8-GFP / +; Or47b-GAL4 / +;* +. (c) *lrp4^{dalek} / Y; UAS-Brp-Short-mStraw, UAS-mCD8-GFP / UAS-Dcr2; Or47b-GAL4 / +;* +. (d) *UAS-Dcr2 / Y; UAS-Brp-Short-mStraw / UAS-lrp4-RNAi 2; Or47b-GAL4 / +;* +. (e) *+ / Y; UAS-Brp-Short-mStraw / +; UAS-LRP4-HA / Or47b-GAL4;* +. (f) *+ / Y; Mz19-GAL4 / +; UAS-Dα7-EGFP / +;* +. (g) *lrp4^{dalek} / Y*; *Mz19-GAL4 / +; UAS-Dα7-EGFP / +;* +. (h) *Control = UAS-Dcr2 / Y; UAS-Brp-Short-mStraw, UAS-mCD8-GFP / +; Or47b-GAL4 / +;* +. *lrp4^{dalek} = lrp4^{dalek} / Y; UAS-Brp-Short-mStraw, UAS-mCD8-GFP / UAS-Dcr2; Or47b-GAL4 / +;* +. *lrp4^{IR-1} = UAS-Dcr2 / Y; UAS-Brp-Short-mStraw / UAS-lrp4-RNAi 1; Or47b-GAL4 / +;* + and *UAS-Dcr2 / Y; UAS-mCD8-GFP / UAS-lrp4-RNAi 1; Or47b-GAL4 / +;* +. *lrp4^{IR-2} = UAS-Dcr2 / Y; UAS-Brp-Short-mStraw / UAS-lrp4-RNAi 2; Or47b-GAL4 / +;* + and *UAS-Dcr2 / Y; UAS-mCD8-GFP / UAS-lrp4-RNAi 2; Or47b-GAL4 / +;* +. *lrp4^{IR-3} = UAS-Dcr2 / Y; UAS-Brp-Short-mStraw / +; Or47b-GAL4 / UAS-lrp4-RNAi 3;* + and *UAS-Dcr2 / Y; UAS-mCD8-GFP / +; Or47b-GAL4 / UAS-lrp4-RNAi 3;* +. *lrp4^{IR-4} = UAS-Dcr2 / Y; UAS-Brp-Short-mStraw / +; Or47b-GAL4 / UAS-lrp4-RNAi 4;* + and *UAS-Dcr2 / Y; UAS-mCD8-GFP / +; Or47b-GAL4 / UAS-lrp4-RNAi 4;* +. *LRP4^{OE} = UAS-Dcr2 / Y; UAS-Brp-Short-mStraw / +; UAS-LRP4-HA / Or47b-GAL4;* + and *UAS-Dcr2 / Y; UAS-mCD8-GFP / +; UAS-LRP4-HA / Or47b-GAL4;* +. (i) *Control = + / Y; Mz19-GAL4, UAS-3xHA-mTDT / +; UAS-Dα7-EGFP / +;* +. *lrp4^{dalek} = lrp4^{dalek} / Y; Mz19-GAL4, UAS-3xHA-mTDT / +; UAS-Dα7-EGFP / +;* +. **Fig. 3**: (a, c-e, f-h) *Control = + / Y; +; +;* +. (b-e, i-q) *lrp4^{dalek} = lrp4^{dalek} / Y; +; +;* +. **Fig. 4**: (a) UAS-Dcr2 / Y; GAD1-GAL4 / UAS-Brp-Short-

mStraw, UAS-mCD8-GFP; +; +. (b) *lrp4^{dalek} / Y; GAD1-GAL4 / UAS-Brp-Short-mStraw, UAS-mCD8-GFP; UAS-Dcr2 / +;* +. (c) *UAS-Dcr2 / Y; GAD1-GAL4 / UAS-Brp-Short-mStraw; UAS-LRP4-HA / +;* +. (d) *Control = UAS-Dcr2 / Y; GAD1-GAL4 / UAS-Brp-Short-mStraw, UAS-mCD8-GFP; +;* +. *lrp4^{dalek} = lrp4^{dalek} / Y; GAD1-GAL4 / UAS-Brp-Short-mStraw, UAS-mCD8-GFP; UAS-Dcr2 / +;* +. *lrp4^{IR-1} = UAS-Dcr2 / Y; GAD1-GAL4, UAS-Brp-Short-mStraw / UAS-lrp4-RNAi 1; +;* + and *UAS-Dcr2 / Y; GAD1-GAL4 / UAS-lrp4-RNAi 1; UAS-mCD8-GFP / +;* +. *lrp4^{IR-2} = UAS-Dcr2 / Y; GAD1-GAL4, UAS-Brp-Short-mStraw / UAS-lrp4-RNAi 2; +;* + and *UAS-Dcr2 / Y; GAD1-GAL4 / UAS-lrp4-RNAi 2; UAS-mCD8-GFP / +;* +. *LRP4^{OE} = UAS-Dcr2 / Y; UAS-Brp-Short-mStraw / GAD1-GAL4; UAS-LRP4-HA / +;* + and *UAS-Dcr2 / Y; UAS-mCD8-GFP / GAD1-GAL4; UAS-LRP4-HA / +;* +. **Fig. 5**: (b) *+ / Y; Mz19-GAL4 / UAS-mCD8-GFP, UAS-Brp-Short-mStraw; UAS-Dcr2 / +;* +. (c) *lrp4^{dalek} / Y; Mz19-GAL4 / UAS-mCD8-GFP, UAS-Brp-Short-mStraw; UAS-Dcr2 / +;* +. (d) *UAS-Dcr2 / Y; UAS-Brp-Short-mStraw, UAS-mCD8-GFP / +; Mz699-GAL4 / +;* +. (e) *lrp4^{dalek} / Y; UAS-Brp-Short-mStraw, UAS-mCD8-GFP / UAS-Dcr2; Mz699-GAL4 / +;* +. (f) Control = *+ / Y; Mz19-GAL4 / UAS-mCD8-GFP, UAS-Brp-Short-mStraw; UAS-Dcr2 / +;* +. *lrp4^{dalek} = lrp4^{dalek} / Y; Mz19-GAL4 / UAS-mCD8-GFP, UAS-Brp-Short-mStraw; UAS-Dcr2 / +;* +. *lrp4^{IR-1} = + / Y; Mz19-GAL4, UAS-mCD8-GFP / UAS-lrp4-RNAi 1; UAS-Brp-Short-mStraw / +;* +. *lrp4^{IR-2} = + / Y; Mz19-GAL4, UAS-mCD8-GFP / UAS-lrp4-RNAi 2; UAS-Brp-Short-mStraw / +;* +. (g) Control = *+ / Y; UAS-Brp-Short-mStraw, UAS-mCD8-GFP / +; Mz699-GAL4 / UAS-Dcr2; +;* +. *lrp4^{dalek} = lrp4^{dalek} / Y; UAS-Brp-Short-mStraw, UAS-mCD8-GFP / +; Mz699-GAL4 / UAS-Dcr2;* +. *lrp4^{IR-1} = + / Y; UAS-mCD8-GFP, UAS-Brp-Short-mStraw / UAS-lrp4-RNAi 1; Mz699-GAL4 / +;* +. *lrp4^{IR-2} = + / Y; UAS-mCD8-GFP, UAS-Brp-Short-mStraw / UAS-lrp4-RNAi 2; Mz699-GAL4 / +;* +. *LRP4^{OE} = + / Y; UAS-mCD8-GFP, UAS-Brp-Short-mStraw / +; Mz699-GAL4 / UAS-LRP4-HA;* +. **Fig. 6**: Column 1 = *pebbled-GAL4 / Y; UAS-mCD8-GFP / +; UAS-mCD8-GFP / +;* +. Column 2 = *+ / Y; UAS-mCD8-GFP / UAS-lrp4-RNAi 1; UAS-mCD8-GFP / +;* +. Column 3 = *+ / Y; UAS-mCD8-GFP / UAS-lrp4-RNAi 2; UAS-mCD8-GFP / +;* +. Column 4 = *+ / Y; UAS-mCD8-GFP / +; UAS-mCD8-GFP / UAS-lrp4-RNAi 3;* +. Column 5 = *+ / Y; UAS-mCD8-GFP / +; UAS-mCD8-GFP / UAS-lrp4-RNAi 4;* +. Column 6 = *pebbled-GAL4 / Y; UAS-lrp4-RNAi 1 / +; UAS-mCD8-GFP / +;* +. Column 7 = *pebbled-GAL4 / Y; UAS-lrp4-RNAi 2 / +; UAS-mCD8-GFP / +;* +. Column 8 = *pebbled-GAL4 / Y; UAS-mCD8-GFP / +; UAS-lrp4-RNAi 3 / +;* +. Column 9 = *pebbled-GAL4 / Y; UAS-mCD8-GFP / +; UAS-lrp4-RNAi 4/ +;* +. Column 10 = *+ / Y; UAS-mCD8-GFP / UAS-GABA$_B$R2-RNAi; UAS-mCD8-GFP / +;* +. Column 11 = *pebbled-GAL4 / Y; UAS-mCD8-GFP / UAS-GABA$_B$R2-RNAi; UAS-mCD8-GFP / +;* +. Column 12 = *+ / Y; UAS-GABA$_B$R2-RNAi / UAS-lrp4-RNAi 2; UAS-mCD8-GFP / +;* +. Column 13 = *pebbled-GAL4 / Y; UAS-lrp4-RNAi 2 / UAS-GABA$_B$R2-RNAi; +;* +. **Fig. 7**: (a) *+ / Y; +; +;* +. (b) *lrp4^{dalek} / Y; +; +;* +. (c) *+ / Y; +; srpk^{atc};* +. (d) *+ / Y; UAS-Brp-Short-mStraw / UAS-venus-SRPK79D-28; Or47b-GAL4 / +;* +. (e) *pebbled-GAL4 / Y; UAS-venus-SRPK79D-28 / +; LRP4-HA / +;* +. (f) *+ / Y; Or47b-GAL4 / UAS-venus-SRPK79D-28; +;* +. (g) *lrp4^{dalek} / Y; Or47b-GAL4 / UAS-venus-SRPK79D-28; +;* +. (h) *Control = + / Y; Or47b-GAL4 / UAS-venus-SRPK79D-28; +;* +. *lrp4^{dalek} = lrp4^{dalek} / Y; Or47b-GAL4 / UAS-venus-SRPK79D-28; +;* +. (i-j) *pebbled-GAL4 / Y; UAS-venus-SRPK79D-28 / +; LRP4-HA / +;* +. **Fig. 8**: (a) *UAS-Dcr2 / Y; UAS-Brp-Short-mStraw, UAS-mCD8-GFP / +; Or47b-GAL4 / +;* +. (b) *UAS-Dcr2 / Y; UAS-Brp-Short-mStraw / +; Or47b-GAL4 / UAS-srpk79D-RNAi;* +. (c) *lrp4^{dalek} / Y; UAS-Brp-Short-mStraw, UAS-mCD8-GFP / UAS-Dcr2; Or47b-GAL4 / +;* +. (d) *lrp4^{dalek} / Y; UAS-Brp-*

Short-mStraw, UAS-mCD8-GFP / +; Or47b-GAL4 / UAS-venus-SRPK79D-1A; +. (e) *Control* = same as (a). *srpk^{RNAi}* = same as (b). srpk^{RNAi} + LRP4^{OE} = *UAS-Dcr2 / Y; Or47b-GAL4 / UAS-srpk79D-RNAi; UAS-LRP4-HA / +;* +. *lrp4^{dalek}* = same as (c). *SRPK^{OE}* = *+ / Y; UAS-Brp-Short-mStraw, UAS-mCD8-GFP / +; Or47b-GAL4 / UAS-venus-SRPK79D-1A;* +. *lrp4^{dalek}* + *SRPK^{OE}* = same as (d). (f) Column 1 = *pebbled-GAL4 / Y; UAS-mCD8-GFP / +; UAS-mCD8-GFP / +;* +. Column 2 = *+ / Y; UAS-srpk79D-RNAi / +; UAS-mCD8-GFP / +;* +. Column 3 = *+ / Y; UAS-mCD8-GFP / UAS-lrp4-RNAi 1; UAS-mCD8-GFP / +;* +. Column 4 = *+ / Y; UAS-mCD8-GFP / +; UAS-mCD8-GFP / UAS-venus-SRPK79D-1A;* +. Column 5 = *+ / Y; UAS-lrp4-RNAi 1 / +; UAS-mCD8-GFP / UAS-venus-SRPK79D-1A;* +. Column 6 = *pebbled-GAL4 / Y; UAS-mCD8-GFP / +; UAS-venus-SRPK79D-1A / +;* +. Column 7 = *pebbled-GAL4 / Y; UAS-srpk79D-RNAi / +; UAS-mCD8-GFP / +;* +. Column 8 = *pebbled-GAL4 / Y; UAS-lrp4-RNAi 1 / +; UAS-mCD8-GFP / +;* +. Column 9 = *pebbled-GAL4 / Y; UAS-lrp4-RNAi 1 / +; UAS-venus-SRPK79D-1A / +;* +. **Supplementary Fig. 2**: (b) + / + = *+; +; +;* +. + / - = *lrp4^{dalek} / +; +; +;* +. - / - = *lrp4^{dalek}; +; +;* +. (c) *+; +; lrp4-GAL4 / UAS-LRP4-HA;* +. (d) *eyFLP$^{3.5}$ / Y; UAS-FRT-STOP-FRT-mCD8-GFP / +; lrp4-GAL4 / +;* +. (e) *+ / Y; GH146-FLP, UAS-FRT-STOP-FRT-mCD8-GFP / +; lrp4-GAL4 / +;* +. **Supplementary Fig. 3**: (a) *+; +; +;* +. (b) *pebbled-GAL4 / Y; UAS-Brp-Short-mStraw / +; +;* +. **Supplementary Fig. 4**: (a,e) *UAS-Dcr2 / Y; UAS-Brp-Short-mStraw, UAS-mCD8-GFP / +; Or47b-GAL4 / +;* +. (b) *UAS-Dcr2 / Y; UAS-Brp-Short-mStraw / UAS-lrp4-RNAi 1; Or47b-GAL4 / +;* +. (c) *UAS-Dcr2 / Y; UAS-Brp-Short-mStraw / +; Or47b-GAL4 / UAS-lrp4-RNAi 3;* +. (d) *UAS-Dcr2 / Y; UAS-Brp-Short-mStraw / +; Or47b-GAL4 / UAS-lrp4-RNAi 4;* +. (f) *lrp4^{dalek} / Y; UAS-Brp-Short-mStraw, UAS-mCD8-GFP / UAS-Dcr2; Or47b-GAL4 / +;* +. (g) *UAS-Dcr2 / Y; UAS-mCD8-GFP / UAS-lrp4-RNAi 1; Or47b-GAL4 / +;* +. (h) *UAS-Dcr2 / Y; UAS-mCD8-GFP / UAS-lrp4-RNAi 2; Or47b-GAL4 / +;* +. (i) *UAS-Dcr2 / Y; UAS-mCD8-GFP / +; Or47b-GAL4 / UAS-lrp4-RNAi 3;* +. (j) *UAS-Dcr2 / Y; UAS-mCD8-GFP / +; Or47b-GAL4 / UAS-lrp4-RNAi 4;* +. (k) *UAS-Dcr2 / Y; UAS-mCD8-GFP / +; UAS-LRP4-HA / Or47b-GAL4;* +. (l) *+ / Y; Mz19-GAL4, UAS-3xHA-mTDT / +; UAS-Dα7-EGFP / +;* +. (m) *lrp4^{dalek} / Y; Mz19-GAL4, UAS-3xHA-mTDT / +; UAS-Dα7-EGFP / +;* +. **Supplementary Fig. 5**: (a) *UAS-Dcr2 / +; UAS-Brp-Short-mStraw, UAS-mCD8-GFP / +; Or47b-GAL4 / +;* +. (b) *UAS-Dcr2 / +; UAS-Brp-Short-mStraw / UAS-lrp4-RNAi 1; Or47b-GAL4 / +;* +. (c) *UAS-Dcr2 / +; UAS-Brp-Short-mStraw / UAS-lrp4-RNAi 2; Or47b-GAL4 / +;* +. (d) *UAS-Dcr2 / +; UAS-Brp-Short-mStraw / +; Or47b-GAL4 / UAS-lrp4-RNAi 3;* +. (e) *UAS-Dcr2 / +; UAS-Brp-Short-mStraw / +; Or47b-GAL4 / UAS-lrp4-RNAi 4;* +. (f) *UAS-Dcr2 / +; UAS-Brp-Short-mStraw, UAS-mCD8-GFP / +; Or47b-GAL4 / +;* +. (g) *UAS-Dcr2 / +; UAS-mCD8-GFP / UAS-lrp4-RNAi 1; Or47b-GAL4 / +;* +. (h) *UAS-Dcr2 / +; UAS-mCD8-GFP / UAS-lrp4-RNAi 2; Or47b-GAL4 / +;* +. (i) *UAS-Dcr2 / +; UAS-mCD8-GFP / +; Or47b-GAL4 / UAS-lrp4-RNAi 3;* +. (j) *UAS-Dcr2 / +; UAS-mCD8-GFP / +; Or47b-GAL4 / UAS-lrp4-RNAi 4;* +. (k) *UAS-Dcr2 / +; UAS-Brp-Short-mStraw / +; UAS-LRP4-HA / Or47b-GAL4;* +. (l) *UAS-Dcr2 / +; UAS-mCD8-GFP / +; UAS-LRP4-HA / Or47b-GAL4;* +. (m) same as **Fig. 2h**. **Supplementary Fig. 6**: (a) *UAS-Dcr2 / Y; AM29-GAL4, UAS-Brp-Short-mStraw / UAS-mCD8-GFP;* +; +. (b) *UAS-Dcr2 / Y; AM29-GAL4, UAS-Brp-Short-mStraw / UAS-lrp4-RNAi 1;* +; +. (c) *UAS-Dcr2 / Y; AM29-GAL4, UAS-Brp-Short-mStraw / UAS-lrp4-RNAi 2;* +; +. (d) *UAS-Dcr2 / Y; UAS-Brp-Short-mStraw, UAS-mCD8-GFP / +; Or88a-GAL4 / +;* +. (e) *UAS-Dcr2 / Y; UAS-Brp-Short-mStraw / UAS-lrp4-RNAi 1; Or88a-GAL4 / +;* +. (f) *UAS-Dcr2 / Y; UAS-Brp-Short-mStraw / UAS-lrp4-RNAi 2; Or88a-GAL4 / +;* +. (g) *UAS-Dcr2 / Y; UAS-Brp-Short-mStraw, UAS-mCD8-GFP / +; Or67d-GAL4 / +;* +.

(h) *UAS-Dcr2 / Y; UAS-Brp-Short-mStraw / UAS-lrp4-RNAi 1; Or67d-GAL4 / +;* +. (i) *UAS-Dcr2 / Y; UAS-Brp-Short-mStraw / UAS-lrp4-RNAi 2; Or67d-GAL4 / +;* +. (j) DL4 and DM6 = same as (a-c). VA1d = same as (d-f). DA1 = same as (g-i). **Supplementary Fig. 7**: (a) *UAS-Dcr2 / Y; UAS-3xHA-mtdT / +; Or67d-GAL4 / UAS-DSyd1-GFP;* +. (b) *UAS-Dcr2 / Y; UAS-lrp4-RNAi 1 / +; Or67d-GAL4 / UAS-DSyd1-GFP;* +. (c) *UAS-Dcr2 / Y; UAS-lrp4-RNAi 2 / +; Or67d-GAL4 / UAS-DSyd1-GFP;* +. (d) Control = as in (a). $lrp4^{IR-1}$ = as in (b). $lrp4^{IR-2}$ = as in (c). **Supplementary Fig. 8**: (a) *+ / Y; Mz19-GAL4 / UAS-mCD8-GFP, UAS-Brp-Short-mStraw; UAS-Dcr2 / +;* +. (b) *+ / Y; Mz19-GAL4, UAS-mCD8-GFP / UAS-lrp4-RNAi 1; UAS-Brp-Short-mStraw / +;* +. (c) *+ / Y; Mz19-GAL4, UAS-mCD8-GFP / UAS-lrp4-RNAi 2; UAS-Brp-Short-mStraw / +;* +. (d) *+ / Y; UAS-Brp-Short-mStraw, UAS-mCD8-GFP / +; Mz699-GAL4 / UAS-Dcr2; +;* +. (e) *+ / Y; UAS-mCD8-GFP, UAS-Brp-Short-mStraw / UAS-lrp4-RNAi 1; Mz699-GAL4 / +;* +. (f) *+ / Y; UAS-mCD8-GFP, UAS-Brp-Short-mStraw / UAS-lrp4-RNAi 2; Mz699-GAL4 / +;* +. (g) *+ / Y; UAS-mCD8-GFP, UAS-Brp-Short-mStraw / +; Mz699-GAL4 / UAS-LRP4-HA;* +. **Supplementary Fig. 9**: (a) *pebbled-GAL4 / Y; UAS-SRPK79D-28 / UAS-Dcr2; +;* +. (b) *pebbled-GAL4 / Y; UAS-Dcr2 / +; UAS-LRP4-HA/ +;* +. (c-d) *pebbled-GAL4 / Y; UAS-SRPK79D-28 / +; UAS-LRP4-HA / +;* +. **Supplementary Fig. 10**: (a) *+; +; +;* +. (b) $lrp4^{dalek}$ */ +; +; +; +*. (c) *+; +;* $srpk^{atc}$ */ +;* +. (d) $lrp4^{dalek}$ */ +; +;* $srpk^{atc}$ */ +;* +. (e) same as in a-d.

AUTHOR CONTRIBUTIONS

TJM conceived of the project, performed experiments, analyzed data, contributed new reagents, and wrote the paper. DJL made the CRISPR mutation in *lrp4* and performed transgenic injections. IEW adapted expansion microscopy for *Drosophila*. TJM and IEW performed expansion microscopy. LL supervised the project. All authors critically reviewed the paper.

ACKNOWLEDGMENTS

We thank Graeme Davis, Kate O'Connor-Giles, and Jing Wang for the kind gift of reagents, the Bloomington Stock Center for flies, and the Developmental Studies Hybridoma Bank (University of Iowa, maintained under the auspices of the NICHD) for antibodies. We acknowledge the Luo Lab and S. Zosimus for fruitful discussions, and T. Clandinin, K. Shen, T. Südhof, K. Beier, N. Berns, L. Denardo Wilke, and J. Lui for critical comments on the manuscript. We also acknowledge T. Clandinin for supporting IEW. This work was supported by grants from the National Institutes of Health (NIH: K99/R00-DC013059 to TJM; R01 DC-005982 to LL). LL is an Investigator of the Howard Hughes Medical Institute.

REFERENCES

1. Vlasits, A. L. *et al.* A Role for Synaptic Input Distribution in a Dendritic Computation of Motion Direction in the Retina. *Neuron* **89,** 1317–30 (2016).
2. Kim, J. S. *et al.* Space-time wiring specificity supports direction selectivity in the retina. *Nature* **509,** 331–6 (2014).
3. Mullins, C., Fishell, G. & Tsien, R. W. Unifying Views of Autism Spectrum Disorders: A Consideration of Autoregulatory Feedback Loops. *Neuron* **89,** 1131–

56 (2016).
4. Bonansco, C. & Fuenzalida, M. Plasticity of Hippocampal Excitatory-Inhibitory Balance: Missing the Synaptic Control in the Epileptic Brain. *Neural Plast.* **2016,** 8607038 (2016).
5. Grant, S. G. N. Synaptopathies: Diseases of the synaptome. *Curr. Opin. Neurobiol.* **22,** 522–529 (2012).
6. Siddiqui, T. J. & Craig, A. M. Synaptic organizing complexes. *Curr. Opin. Neurobiol.* **21,** 132–43 (2011).
7. Takahashi, H. & Craig, A. M. Protein tyrosine phosphatases PTPδ, PTPσ, and LAR: presynaptic hubs for synapse organization. *Trends Neurosci.* **36,** 522–34 (2013).
8. Mosca, T. J. On the Teneurin track: a new synaptic organization molecule emerges. *Front. Cell. Neurosci.* **9,** 1–14 (2015).
9. de Wit, J. & Ghosh, A. Specification of synaptic connectivity by cell surface interactions. *Nat. Rev. Neurosci.* **17,** 4 (2016).
10. Südhof, T. C. Neuroligins and neurexins link synaptic function to cognitive disease. *Nature* **455,** 903–11 (2008).
11. Hruska, M. & Dalva, M. B. Ephrin regulation of synapse formation, function and plasticity. *Mol. Cell. Neurosci.* **50,** 35–44 (2012).
12. Weatherbee, S. D., Anderson, K. V & Niswander, L. A. LDL-receptor-related protein 4 is crucial for formation of the neuromuscular junction. *Development* **133,** 4993–5000 (2006).
13. Kim, N. *et al.* Lrp4 is a receptor for Agrin and forms a complex with MuSK. *Cell* **135,** 334–342 (2008).
14. Barik, A. *et al.* LRP4 Is Critical for Neuromuscular Junction Maintenance. *J. Neurosci.* **34,** 13892–905 (2014).
15. Yumoto, N., Kim, N. & Burden, S. J. Lrp4 is a retrograde signal for presynaptic differentiation at neuromuscular synapses. *Nature* **489,** 438–42 (2012).
16. Wu, H. *et al.* Distinct roles of muscle and motoneuron LRP4 in neuromuscular junction formation. *Neuron* **75,** 94–107 (2012).
17. Daniels, M. P. The role of agrin in synaptic development, plasticity and signaling in the central nervous system. *Neurochem. Int.* **61,** 848–853 (2012).
18. Gomez, A. M., Froemke, R. C. & Burden, S. J. Synaptic plasticity and cognitive function are disrupted in the absence of Lrp4. *Elife* **3,** (2014).
19. Pohlkamp, T. *et al.* Lrp4 Domains Differentially Regulate Limb/Brain Development and Synaptic Plasticity. *PLoS One* **10,** e0116701 (2015).
20. Sun, X. *et al.* Lrp4 in astrocytes modulates glutamatergic transmission. *Nat. Neurosci.* 1–12 (2016). doi:10.1038/nn.4326
21. Adams, M. D. *et al.* The genome sequence of Drosophila melanogaster. *Science* **287,** 2185–95 (2000).
22. Chintapalli, V. R., Wang, J. & Dow, J. a T. Using FlyAtlas to identify better Drosophila melanogaster models of human disease. *Nat. Genet.* **39,** 715–20 (2007).
23. Wilson, R. I. Early olfactory processing in Drosophila: mechanisms and principles. *Annu. Rev. Neurosci.* **36,** 217–41 (2013).
24. Mosca, T. J. & Luo, L. Synaptic organization of the Drosophila antennal lobe and

its regulation by the Teneurins. *Elife* **3,** e03726 (2014).
25. Wagh, D. A. *et al.* Bruchpilot, a protein with homology to ELKS/CAST, is required for structural integrity and function of synaptic active zones in Drosophila. *Neuron* **49,** 833–844 (2006).
26. Chen, F., Tillberg, P. W. & Boyden, E. S. Optical imaging. Expansion microscopy. *Science* **347,** 543–8 (2015).
27. Tillberg, P. W. *et al.* Protein-retention expansion microscopy of cells and tissues labeled using standard fluorescent proteins and antibodies. *Nat. Biotechnol.* 1–9 (2016). doi:10.1038/nbt.3625
28. Shyamala, B. V & Chopra, A. Drosophila melanogaster chemosensory and muscle development: identification and properties of a novel allele of scalloped and of a new locus, SG18.1, in a Gal4 enhancer trap screen. *J. Genet.* **78,** 87–97 (1999).
29. Mosca, T. J., Hong, W., Dani, V. S., Favaloro, V. & Luo, L. Trans-synaptic Teneurin signalling in neuromuscular synapse organization and target choice. *Nature* **484,** 237–41 (2012).
30. Jepson, J. E. C. *et al.* Regulation of synaptic development and function by the Drosophila PDZ protein Dyschronic. *Development* 1–10 (2014). doi:10.1242/dev.109538
31. Li, J., Ashley, J., Budnik, V. & Bhat, M. A. Crucial role of Drosophila neurexin in proper active zone apposition to postsynaptic densities, synaptic growth, and synaptic transmission. *Neuron* **55,** 741–755 (2007).
32. Robinow, S. & White, K. The locus elav of Drosophila melanogaster is expressed in neurons at all developmental stages. *Dev. Biol.* **126,** 294–303 (1988).
33. Xiong, W. C., Okano, H., Patel, N. H., Blendy, J. A. & Montell, C. repo encodes a glial-specific homeo domain protein required in the Drosophila nervous system. *Genes Dev.* **8,** 981–94 (1994).
34. Fouquet, W. *et al.* Maturation of active zone assembly by Drosophila Bruchpilot. *J Cell Biol* **186,** 129–145 (2009).
35. Leiss, F. *et al.* Characterization of dendritic spines in the Drosophila central nervous system. *Dev. Neurobiol.* **69,** 221–234 (2009).
36. Tobin, W. F., Wilson, R. I. & Lee, W.-C. A. Wiring variations that enable and constrain neural computation in a sensory microcircuit. *bioRxiv* (2017).
37. Gratz, S. J. *et al.* Genome engineering of Drosophila with the CRISPR RNA-guided Cas9 nuclease. *Genetics* (2013). doi:10.1534/genetics.113.152710
38. Owald, D. *et al.* Cooperation of Syd-1 with Neurexin synchronizes pre- with postsynaptic assembly. *Nat. Neurosci.* (2012). doi:10.1038/nn.3183
39. Craig, A. M. & Kang, Y. Neurexin-neuroligin signaling in synapse development. *Curr. Opin. Neurobiol.* **17,** 43–52 (2007).
40. Chen, Y. *et al.* Cell-type-Specific Labeling of Synapses In Vivo through Synaptic Tagging with Recombination. *Neuron* **81,** 280–93 (2014).
41. Rybak, J. *et al.* Synaptic circuitry of identified neurons in the antennal lobe of Drosophila melanogaster. *J. Comp. Neurol.* **524,** 1920–56 (2016).
42. Ng, M. *et al.* Transmission of olfactory information between three populations of neurons in the antennal lobe of the fly. *Neuron* **36,** 463–74 (2002).
43. Mehren, J. E. & Griffith, L. C. Cholinergic neurons mediate CaMKII-dependent

enhancement of courtship suppression. *Learn. Mem.* **13,** 686–9 (2006).
44. Heimbeck, G., Bugnon, V., Gendre, N., Keller, A. & Stocker, R. F. A central neural circuit for experience-independent olfactory and courtship behavior in Drosophila melanogaster. *Proc. Natl. Acad. Sci. U. S. A.* **98,** 15336–41 (2001).
45. Berdnik, D., Chihara, T., Couto, A. & Luo, L. Wiring stability of the adult Drosophila olfactory circuit after lesion. *J. Neurosci.* **26,** 3367–76 (2006).
46. Liang, L. *et al.* GABAergic projection neurons route selective olfactory inputs to specific higher-order neurons. *Neuron* **79,** 917–31 (2013).
47. Lai, S.-L., Awasaki, T., Ito, K. & Lee, T. Clonal analysis of Drosophila antennal lobe neurons: diverse neuronal architectures in the lateral neuroblast lineage. *Development* **135,** 2883–2893 (2008).
48. Potter, C. J., Tasic, B., Russler, E. V, Liang, L. & Luo, L. The Q system: a repressible binary system for transgene expression, lineage tracing, and mosaic analysis. *Cell* **141,** 536–548 (2010).
49. Larsson, M. C. *et al.* Or83b encodes a broadly expressed odorant receptor essential for Drosophila olfaction. *Neuron* **43,** 703–14 (2004).
50. Min, S., Ai, M., Shin, S. A. & Suh, G. S. B. Dedicated olfactory neurons mediating attraction behavior to ammonia and amines in Drosophila. *Proc. Natl. Acad. Sci. U. S. A.* **110,** E1321-9 (2013).
51. Root, C. M. *et al.* A presynaptic gain control mechanism fine-tunes olfactory behavior. *Neuron* **59,** 311–21 (2008).
52. Olsen, S. R. & Wilson, R. I. Lateral presynaptic inhibition mediates gain control in an olfactory circuit. *Nature* **452,** 956–960 (2008).
53. DiAntonio, A. *et al.* Identification and characterization of Drosophila genes for synaptic vesicle proteins. *J Neurosci* **13,** 4924–4935 (1993).
54. Johnson, E. L., Fetter, R. D. & Davis, G. W. Negative regulation of active zone assembly by a newly identified SR protein kinase. *PLoS Biol.* **7,** e1000193–e1000193 (2009).
55. Nieratschker, V. *et al.* Bruchpilot in ribbon-like axonal agglomerates, behavioral defects, and early death in SRPK79D kinase mutants of Drosophila. *PLoS Genet.* **5,** e1000700 (2009).
56. Gindhart, J. G., Desai, C. J., Beushausen, S., Zinn, K. & Goldstein, L. S. Kinesin light chains are essential for axonal transport in Drosophila. *J. Cell Biol.* **141,** 443–454 (1998).
57. Söderberg, O. *et al.* Direct observation of individual endogenous protein complexes in situ by proximity ligation. *Nat. Methods* **3,** 995–1000 (2006).
58. Greenwood, C. *et al.* Proximity assays for sensitive quantification of proteins. *Biomol. Detect. Quantif.* **4,** 10–16 (2015).
59. Wang, S. *et al.* Detection of in situ protein-protein complexes at the Drosophila larval neuromuscular junction using proximity ligation assay. *J. Vis. Exp.* 52139 (2015). doi:10.3791/52139
60. Sweeney, L. B. *et al.* Temporal target restriction of olfactory receptor neurons by Semaphorin-1a/PlexinA-mediated axon-axon interactions. *Neuron* **53,** 185–200 (2007).
61. Zhang, B. *et al.* LRP4 serves as a coreceptor of agrin. *Neuron* **60,** 285–297 (2008).

62. Badawy, R. A. B., Freestone, D. R., Lai, A. & Cook, M. J. Epilepsy: Ever-changing states of cortical excitability. *Neuroscience* **222,** 89–99 (2012).
63. Yizhar, O. *et al.* Neocortical excitation/inhibition balance in information processing and social dysfunction. *Nature* **477,** 171–8 (2011).
64. Nelson, S. B. & Valakh, V. Excitatory/Inhibitory Balance and Circuit Homeostasis in Autism Spectrum Disorders. *Neuron* **87,** 684–98 (2015).
65. Ziv, N. E. & Fisher-Lavie, A. Presynaptic and postsynaptic scaffolds: dynamics fast and slow. *Neuroscientist* **20,** 439–52 (2014).
66. Sheng, M. & Kim, E. The postsynaptic organization of synapses. *Cold Spring Harb. Perspect. Biol.* **3,** a005678 (2011).
67. Graf, E. R., Zhang, X., Jin, S.-X., Linhoff, M. W. & Craig, A. M. Neurexins induce differentiation of GABA and glutamate postsynaptic specializations via neuroligins. *Cell* **119,** 1013–26 (2004).
68. Choii, G. & Ko, J. Gephyrin: a central GABAergic synapse organizer. *Exp. Mol. Med.* **47,** e158 (2015).
69. Takahashi, H. *et al.* Selective control of inhibitory synapse development by Slitrk3-PTPδ trans-synaptic interaction. *Nat. Neurosci.* **15,** 389–98, S1-2 (2012).
70. de Wit, J. *et al.* LRRTM2 interacts with Neurexin1 and regulates excitatory synapse formation. *Neuron* **64,** 799–806 (2009).
71. de Wit, J. *et al.* Unbiased discovery of glypican as a receptor for LRRTM4 in regulating excitatory synapse development. *Neuron* **79,** 696–711 (2013).
72. Siddiqui, T. J. *et al.* An LRRTM4-HSPG complex mediates excitatory synapse development on dentate gyrus granule cells. *Neuron* **79,** 680–95 (2013).
73. Pinan-Lucarré, B. *et al.* C. elegans Punctin specifies cholinergic versus GABAergic identity of postsynaptic domains. *Nature* **511,** 466–470 (2014).
74. Tu, H., Pinan-Lucarré, B., Ji, T., Jospin, M. & Bessereau, J.-L. C. elegans Punctin Clusters GABAA Receptors via Neuroligin Binding and UNC-40/DCC Recruitment. *Neuron* **86,** 1407–1419 (2015).
75. Maro, G. S. *et al.* MADD-4/Punctin and Neurexin Organize C. elegans GABAergic Postsynapses through Neuroligin. *Neuron* **86,** 1420–1432 (2015).
76. Allen, N. J. *et al.* Astrocyte glypicans 4 and 6 promote formation of excitatory synapses via GluA1 AMPA receptors. *Nature* (2012). doi:10.1038/nature11059
77. Biesemann, C. *et al.* Proteomic screening of glutamatergic mouse brain synaptosomes isolated by fluorescence activated sorting. *EMBO J.* **33,** 157–70 (2014).
78. Boyken, J. *et al.* Molecular profiling of synaptic vesicle docking sites reveals novel proteins but few differences between glutamatergic and GABAergic synapses. *Neuron* **78,** 285–97 (2013).
79. Liu, W. W. & Wilson, R. I. Glutamate is an inhibitory neurotransmitter in the Drosophila olfactory system. *Proc. Natl. Acad. Sci. U. S. A.* **110,** 10294–9 (2013).
80. Zhang, W., Coldefy, A.-S., Hubbard, S. R. & Burden, S. J. Agrin binds to the N-terminal region of Lrp4 protein and stimulates association between Lrp4 and the first immunoglobulin-like domain in muscle-specific kinase (MuSK). *J. Biol. Chem.* **286,** 40624–40630 (2011).
81. Tian, Q.-B. *et al.* Interaction of LDL receptor-related protein 4 (LRP4) with postsynaptic scaffold proteins via its C-terminal PDZ domain-binding motif, and its

regulation by Ca/calmodulin-dependent protein kinase II. *Eur. J. Neurosci.* **23,** 2864–76 (2006).
82. Zhou, Z. & Fu, X.-D. Regulation of splicing by SR proteins and SR protein-specific kinases. *Chromosoma* **122,** 191–207 (2013).
83. Lein, E. S. *et al.* Genome-wide atlas of gene expression in the adult mouse brain. *Nature* **445,** 168–176 (2007).
84. Tsivgoulis, G. *et al.* Double seronegative myasthenia gravis with low density lipoprotein-4 (LRP4) antibodies presenting with isolated ocular symptoms. *J. Neurol. Sci.* **346,** 328–330 (2014).
85. Tzartos, J. S. *et al.* LRP4 antibodies in serum and CSF from amyotrophic lateral sclerosis patients. *Ann. Clin. Transl. Neurol.* **1,** 80–7 (2014).
86. Shen, C. *et al.* Antibodies against low-density lipoprotein receptor-related protein 4 induce myasthenia gravis. *J. Clin. Invest.* **123,** 5190–202 (2013).
87. Ringholz, G. M. *et al.* Prevalence and patterns of cognitive impairment in sporadic ALS. *Neurology* **65,** 586–590 (2005).
88. Bellen, H. J. *et al.* The Drosophila gene disruption project: progress using transposons with distinctive site specificities. *Genetics* **188,** 731–743 (2011).
89. Pfeiffer, B. D. *et al.* Tools for neuroanatomy and neurogenetics in Drosophila. *Proc. Natl. Acad. Sci. U. S. A.* **105,** 9715–9720 (2008).
90. Vosshall, L. B., Wong, a M. & Axel, R. An olfactory sensory map in the fly brain. *Cell* **102,** 147–59 (2000).
91. Kurtovic, A., Widmer, A. & Dickson, B. J. A single class of olfactory neurons mediates behavioural responses to a Drosophila sex pheromone. *Nature* **446,** 542–546 (2007).
92. Endo, K., Aoki, T., Yoda, Y., Kimura, K. & Hama, C. Notch signal organizes the Drosophila olfactory circuitry by diversifying the sensory neuronal lineages. *Nat. Neurosci.* **10,** 153–160 (2007).
93. Jefferis, G. S. X. E. *et al.* Developmental origin of wiring specificity in the olfactory system of Drosophila. *Development* **131,** 117–130 (2004).
94. Robinson, I. M., Ranjan, R. & Schwarz, T. L. Synaptotagmins I and IV promote transmitter release independently of Ca(2+) binding in the C(2)A domain. *Nature* **418,** 336–340 (2002).
95. Owald, D. *et al.* A Syd-1 homologue regulates pre- and postsynaptic maturation in Drosophila. *J. Cell Biol.* **188,** 565–579 (2010).
96. Lee, T. & Luo, L. Mosaic analysis with a repressible cell marker for studies of gene function in neuronal morphogenesis. *Neuron* **22,** 451–461 (1999).
97. Hong, W. *et al.* Leucine-rich repeat transmembrane proteins instruct discrete dendrite targeting in an olfactory map. *Nat. Neurosci.* **12,** 1542–1550 (2009).
98. Dietzl, G. *et al.* A genome-wide transgenic RNAi library for conditional gene inactivation in Drosophila. *Nature* **448,** 151–156 (2007).
99. Chotard, C., Leung, W. & Salecker, I. glial cells missing and gcm2 Cell Autonomously Regulate Both Glial and Neuronal Development in the Visual System of Drosophila. *Neuron* **48,** 237–251 (2005).
100. Wu, J. S. & Luo, L. A protocol for dissecting Drosophila melanogaster brains for live imaging or immunostaining. *Nat. Protoc.* **1,** 2110–2115 (2006).
101. Mosca, T. J. & Schwarz, T. L. The nuclear import of Frizzled2-C by Importins-

beta11 and alpha2 promotes postsynaptic development. *Nat. Neurosci.* **13,** 935–43 (2010).
102. Laissue, P. P. *et al.* Three-dimensional reconstruction of the antennal lobe in Drosophila melanogaster. *J. Comp. Neurol.* **405,** 543–552 (1999).
103. Mackler, J. M., Drummond, J. a, Loewen, C. a, Robinson, I. M. & Reist, N. E. The C(2)B Ca(2+)-binding motif of synaptotagmin is required for synaptic transmission in vivo. *Nature* **418,** 340–4 (2002).
104. Iwai, Y. *et al.* Axon patterning requires DN-cadherin, a novel neuronal adhesion receptor, in the Drosophila embryonic CNS. *Neuron* **19,** 77–89 (1997).
105. Takagawa, K. & Salvaterra, P. Analysis of choline acetyltransferase protein in temperature sensitive mutant flies using newly generated monoclonal antibody. *Neurosci. Res.* **24,** 237–243 (1996).
106. O'Neill, E. M., Rebay, I., Tjian, R. & Rubin, G. M. The activities of two Ets-related transcription factors required for Drosophila eye development are modulated by the Ras/MAPK pathway. *Cell* **78,** 137–147 (1994).
107. Alfonso, T. B. & Jones, B. W. gcm2 promotes glial cell differentiation and is required with glial cells missing for macrophage development in Drosophila. *Dev. Biol.* **248,** 369–383 (2002).
108. Daniels, R. W., Gelfand, M. V., Collins, C. A. & DiAntonio, A. Visualizing glutamatergic cell bodies and synapses in Drosophila larval and adult CNS. *J. Comp. Neurol.* **508,** 131–52 (2008).
109. Hussain, M. M. Structural, biochemical and signaling properties of the low-density lipoprotein receptor gene family. *Front. Biosci.* **6,** D417-28 (2001).
110. Stockinger, P., Kvitsiani, D., Rotkopf, S., Tirián, L. & Dickson, B. J. Neural circuitry that governs Drosophila male courtship behavior. *Cell* **121,** 795–807 (2005).

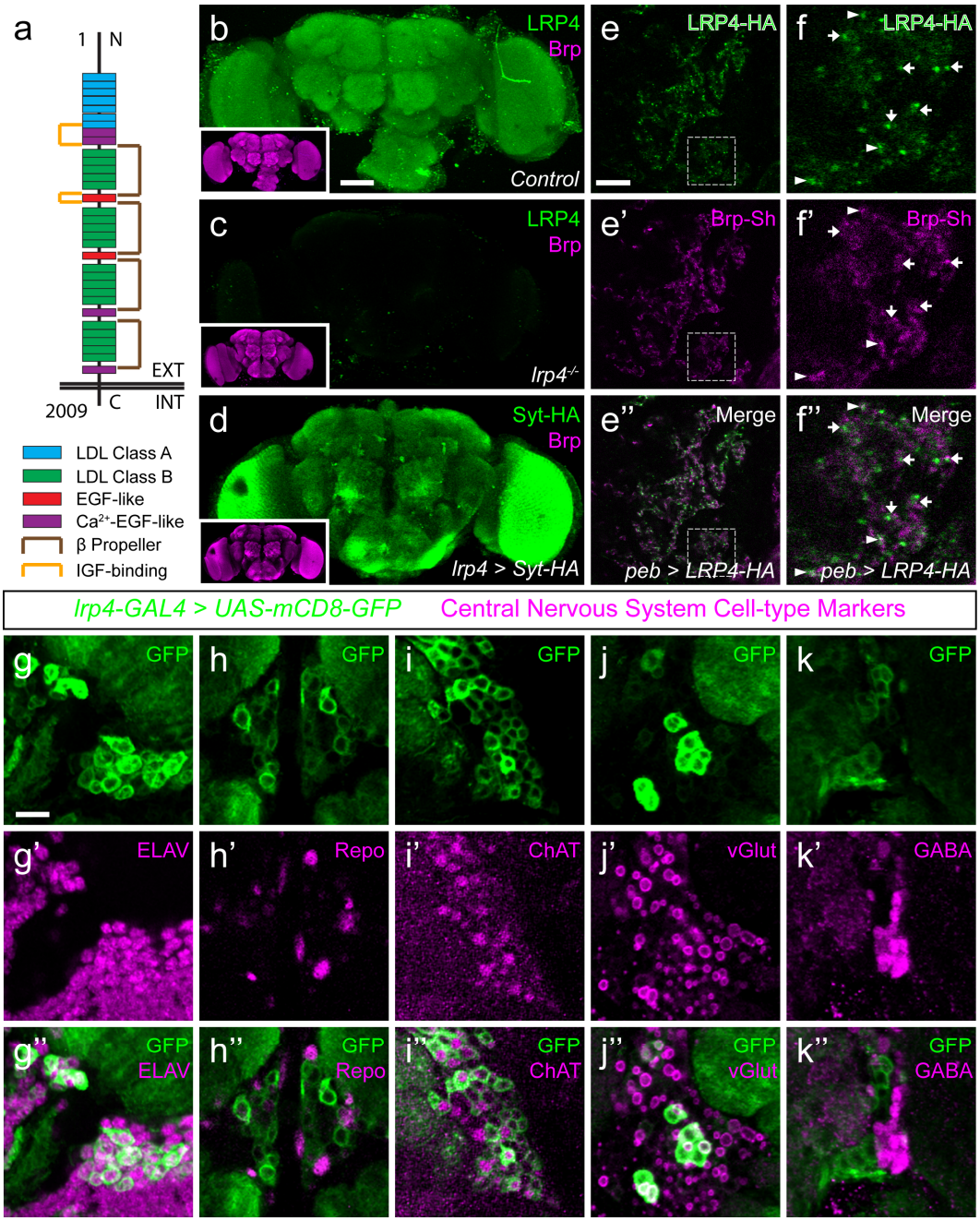

Figure 1. LRP4 is a synaptic protein expressed in excitatory neurons.
(a) Domain structure of *Drosophila* LRP4. Numbers indicate amino acids. EXT, extracellular side. INT, intracellular side.
(b) Representative confocal image stack of a control *Drosophila* brain stained with antibodies against endogenous LRP4 (green) and Bruchpilot (inset, magenta) demonstrating expression throughout the brain.
(c) Representative confocal image stack of an *lrp4*^{dalek} null brain stained with antibodies against LRP4 (green) and Brp (inset, magenta) demonstrating antibody specificity.
(d) Representative confocal image of a *Drosophila* brain expressing *UAS-Syt-HA* via *lrp4-GAL4* and stained with antibodies to HA (D, green) and N-Cadherin (inset, magenta). The

expression pattern resembles that of endogenous LRP4, supporting the specificity of *lrp4-GAL4*.
(e) Representative single slice within a single antennal lobe glomerulus of a brain processed for expansion microscopy (proExM) expressing LRP4-HA and Brp-Short-mStraw in all ORNs via *pebbled-GAL4* and stained with antibodies to HA (e, e", green) and mStraw (e'-e", magenta). LRP4 localizes to synaptic neuropil regions.
(f) High magnification image of the region bounded by dashed lines in (e) and stained as above. Arrows indicate LRP4-HA localization adjacent to / not directly overlapping with Bruchpilot-Short. Arrowheads indicate overlapping LRP4-HA and Brp-Short localization.
(g-k) Representative high magnification confocal stack images of neuronal cell bodies surrounding the antennal lobe in animals expressing *UAS-mCD8-GFP* via *lrp4-GAL4* and stained for antibodies against GFP (g-k, green) and other cell-type markers (g'-k', magenta). Merge channels (g''-k'') show colocalization of *lrp4* with the neuronal marker ELAV (g'') but not the glial cell marker Repo (h''). Neurons positive for *lrp4* show colocalization with choline acetyltransferase (ChAT, i''), and the vesicular glutamate transporter (vGlut, j''), but little to no colocalization with the inhibitory neurotransmitter GABA (k''), suggesting that *lrp4*-positive cells are largely excitatory neurons. The percentage of GFP-positive cells that are ALSO positive for the cell-type specific marker are as follows: Elav = 99.50 ± 0.19% overlap; Repo = 0.38 ± 0.18% overlap; ChAT = 59.13 ± 2.48% overlap; vGlut = 22.38 ± 1.28% overlap; GABA = 0.25 ± 0.16% overlap. For all cases, n = 8 animals, ≥ 200 cells per animal. Values = mean ± s.e.m.
Scale bars = 50 μm (b-d), 150 μm (b-d, insets), 25 μm (e-f), 10 μm (g-k).

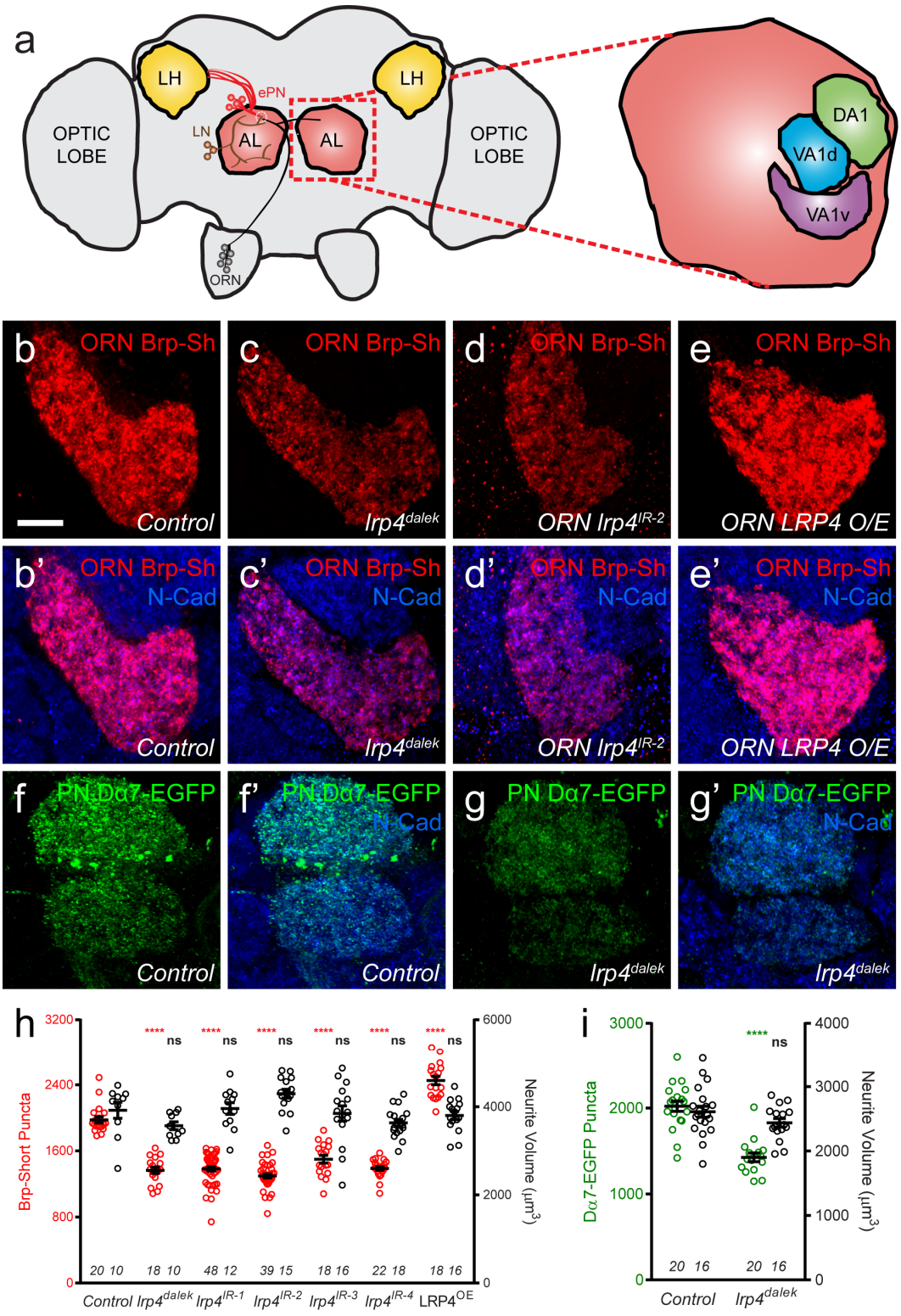

Figure 2. LRP4 perturbation in excitatory neurons alters synapse number.
(a) Schematic diagram of the fly brain with major regions labeled and the olfactory regions examined in this study shaded in red (AL, antennal lobe) or yellow (LH, the lateral horn). Olfactory receptor neurons (ORNs, black), excitatory projection neurons (ePNs, red), and

local interneurons (LNs, brown) are indicated. White dashed lines represent a glomerulus. Magnification: the antennal lobe region with the three glomeruli examined here highlighted: DA1 (green), VA1d (blue), and VA1v (purple).
(b-e) Representative high magnification confocal stack images of VA1v ORN axon terminals in the VA1v glomerulus of males expressing Brp-Short-mStraw and stained with antibodies against mStraw (red) and N-Cadherin (blue). Loss of *lrp4* (*lrp4*^{dalek}) and RNAi against *lrp4* expressed only in ORNs (*ORN lrp4*$^{IR-2}$) show fewer Brp-Short-mStraw puncta while LRP4 overexpression in ORNs (*ORN LRP4 OE*) increases the number of Brp-Short-mStraw puncta.
(f-g) Representative high magnification confocal maximum intensity projections of DA1 and VA1d PN dendrites in males expressing Dα7-EGFP, a tagged acetylcholine receptor subunit. Loss of *lrp4 (lrp4*^{dalek}*)* also results in fewer Dα7-EGFP puncta.
(h) Quantification of Brp-Short-mStraw puncta (red, left axis) and neurite volume (black, right axis) in VA1v ORNs.
(i) Quantification of Dα7-EGFP puncta (green, left axis) and neurite volume (black, right axis). In both cases, *n* (antennal lobes) is noted at the bottom of each column.
****, $p < 0.0001$; ***, $p < 0.001$; ns, not significant. Statistical comparisons (one-way ANOVA with correction for multiple comparisons) are with control. Error bars in this and all subsequent figures represent mean ± s.e.m.
Scale bars = 10 μm.

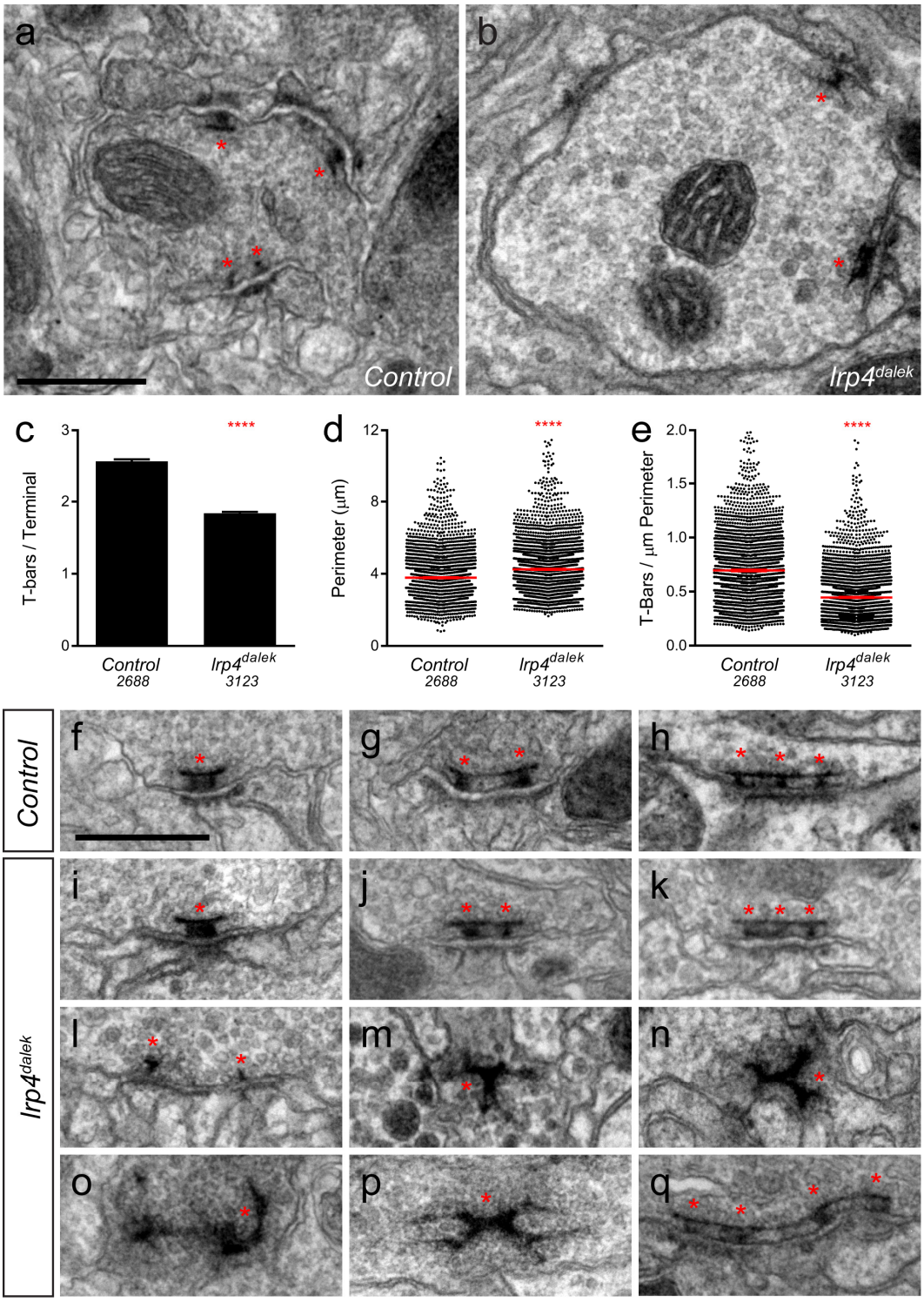

Figure 3. Loss of LRP4 causes defects in T-bar number and morphology.
(a-b) Representative transmission electron micrographs of putative ORN terminal in *Control* (a) and *lrp4*^{dalek} adult antennal lobes. Loss of *lrp4* results in fewer observed T-bar profiles (asterisk) and a larger terminal perimeter. Scale bar = 1 µm.

(c) Quantification of T-bar profiles per terminal in *Control* and *lrp4*^{dalek} terminals. Loss of LRP4 results in a 31% reduction of T-bars.
(d) Quantification of terminal perimeter in *Control* and *lrp4*^{dalek} adults. Mutant terminals have a 13% greater perimeter than control terminals.
(e) Quantification of the T-bar density per µm of terminal perimeter. Loss of LRP4 causes a 36% reduction in T-bar density when the increased terminal perimeter is accounted for. For (c-e), Control has n = 5 animals, 2,688 terminals and *lrp4*^{dalek} has n = 3 animals, 3,123 terminals. The number of terminals measured is listed below the genotype. ****, $p < 0.0001$. Statistical comparisons (two-tailed Student's t-test) are done between genotypes.
(f-h) Representative transmission electron micrographs of individual T-bar profiles (asterisk) in *control* adults. Single (f), double (g), and triple (h) profiles are readily visible.
(i-q) Representative transmission electron micrographs of individual T-bar profiles in *lrp4*^{dalek} adults. As in control flies, single (i), double (j) and triple (k) T-bar profiles were visible. The majority of T-bars, however, demonstrated morphology defects including those that lacked table tops (l), were detached from the membrane (m-n), were misshapen (n-p), and profiles containing 4 or more connected T-bars (q). These all represent morphological defects that are not observed (or very rarely observed) in control adults. Scale bar = 200 nm.

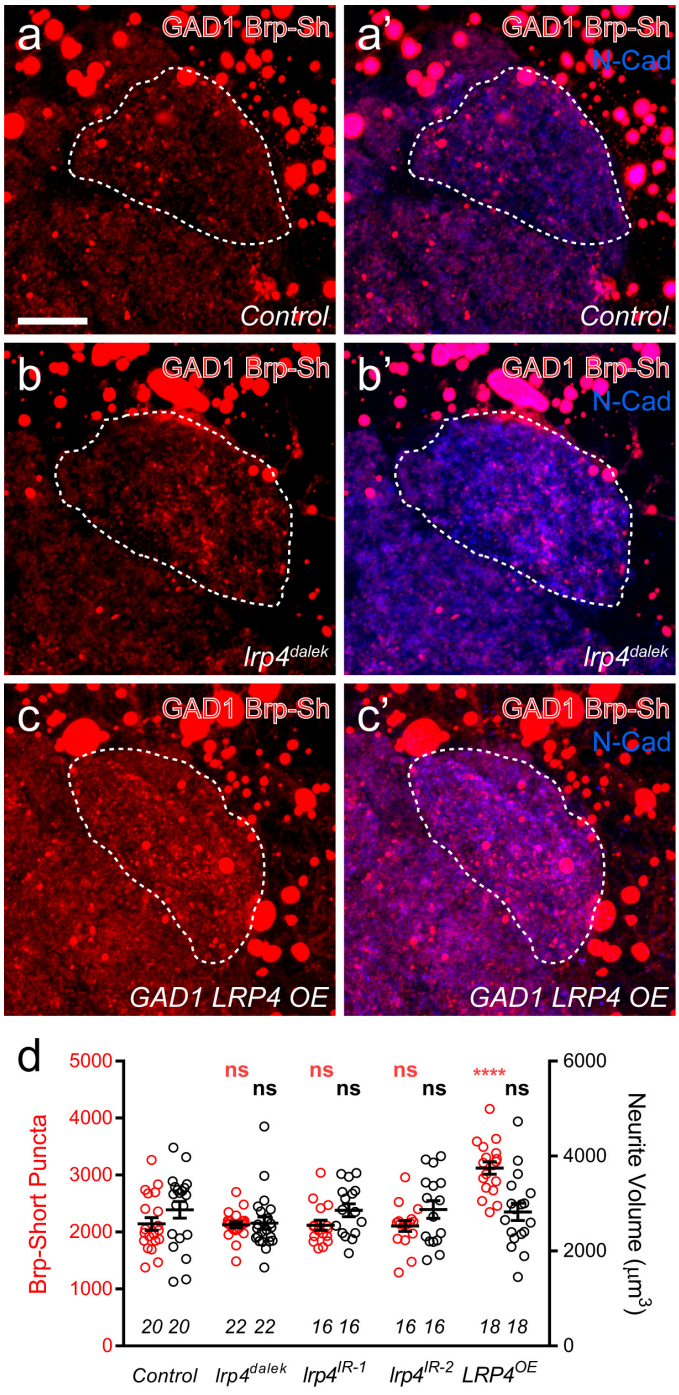

Figure 4. Effects of LRP4 perturbation on inhibitory neuron synapse formation. (a-c) Representative high magnification confocal maximum intensity projections of GAD1-positive inhibitory neurons, which project to the DA1 glomerulus (dashed line), in males expressing Brp-Short-mStraw and stained with antibodies against mStraw (red) and N-Cadherin (blue). Due to the proximity of inhibitory neuron cell bodies to the antennal lobe, saturated somatic signal is observed. Loss of *lrp4* (*lrp4*^{dalek}) does not affect puncta number but overexpression of LRP4 (*GAD1 LRP4 OE*) increases Brp-Short puncta.

(d) Quantification of Brp-Short-mStraw puncta (red, left axis) and neurite volume (black, right axis) in GAD1 neurons. Neither loss of *lrp4* nor RNAi against *lrp4* expressed in inhibitory neurons affects puncta number or neurite volume. *n* (antennal lobes) is noted at the bottom of each column.
****, $p < 0.0001$; ***, $p < 0.001$; ns, not significant. Statistical comparisons (one-way ANOVA with correction for multiple comparisons) are with control.
Scale bars = 10 μm.

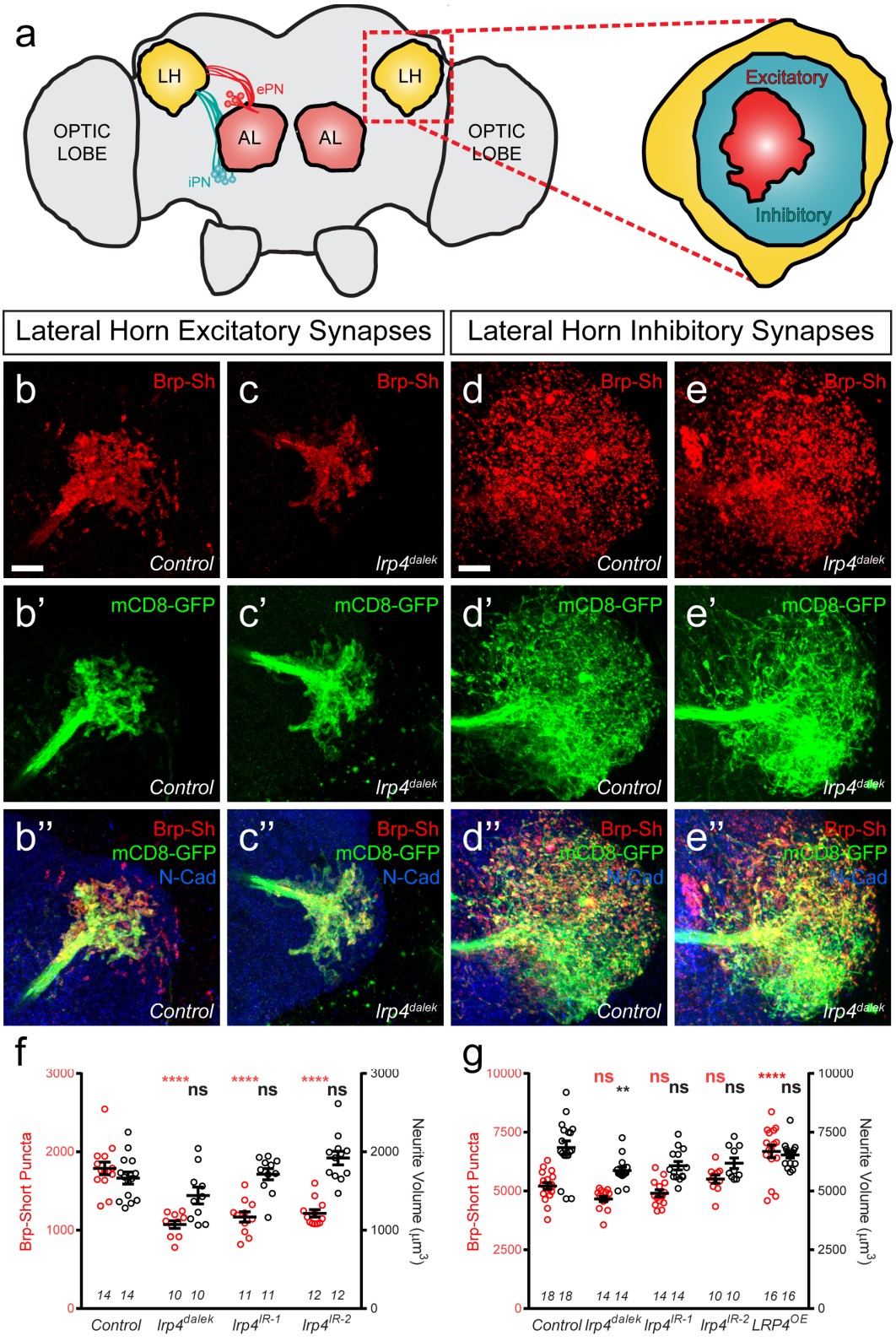

Figure 5. LRP4 perturbations similarly affect higher order olfactory centers.
(a) Schematic diagram of the fly brain with major regions labeled and the olfactory regions examined in this study shaded in red (AL, antennal lobe) or yellow (LH, the lateral horn).

Excitatory projection neuron (ePN, dark red) and inhibitory projection neuron (iPN, teal) axons are indicated. Magnification: the lateral horn region with the regions innervated by excitatory Mz19-positive projection neuron axons (ePNs, dark red) and inhibitory Mz699-positive projection neuron axons (iPNs, teal) examined here highlighted.
(b-c) Representative high magnification confocal maximum intensity projections of *Mz19-GAL4* positive PN axon terminals in the lateral horn in males expressing Brp-Short-mStraw and mCD8-GFP and stained for antibodies against mStraw (red), GFP (green), and N-Cadherin (blue). Loss of *lrp4* (b, $lrp4^{dalek}$) reduces synapse number compared to control (a).
(d-e) Representative high magnification confocal maximum intensity projections of *Mz699-GAL4* positive inhibitory projection neuron (iPN) axon terminals in the lateral horn in males expressing Brp-Short-mStraw and mCD8-GFP and stained for antibodies against mStraw (red), GFP (green), and N-Cadherin (blue). Loss of *lrp4* (d, $lrp4^{dalek}$) does not affect synapse number compared to control (d).
(f) Quantification of Brp-Short-mStraw puncta (red, left axis) and neurite volume (black, right axis) in Mz19-positive excitatory projection neurons. Loss of *lrp4* and RNAi against *lrp4* expressed in those neurons reduces puncta number but leaves neurite volume unaffected. The similar reduction in puncta number between mutants and PN-specific RNAi reveals the cell autonomous nature of the *lrp4* phenotype.
(g) Quantification of Brp-Short-mStraw puncta (red, left axis) and neurite volume (black, right axis) in Mz699-positive inhibitory projection neurons. Neither loss of *lrp4* nor *lrp4* RNAi expressed in those neurons affects puncta number, similar to inhibitory neurons in the antennal lobe. Loss of *lrp4* reduces neurite volume by 11% but RNAi does not. Overexpression of LRP4 in these neurons (*LRP4 OE*) results in a 28% increase in the number of Brp-Short puncta. *n* (antennal lobes) is noted at the bottom of each column.
****, $p < 0.0001$; **, $p < 0.01$; ns, not significant. Statistical comparisons (one way ANOVA with correction for multiple comparisons) are with control.
Scale bars = 10 μm.

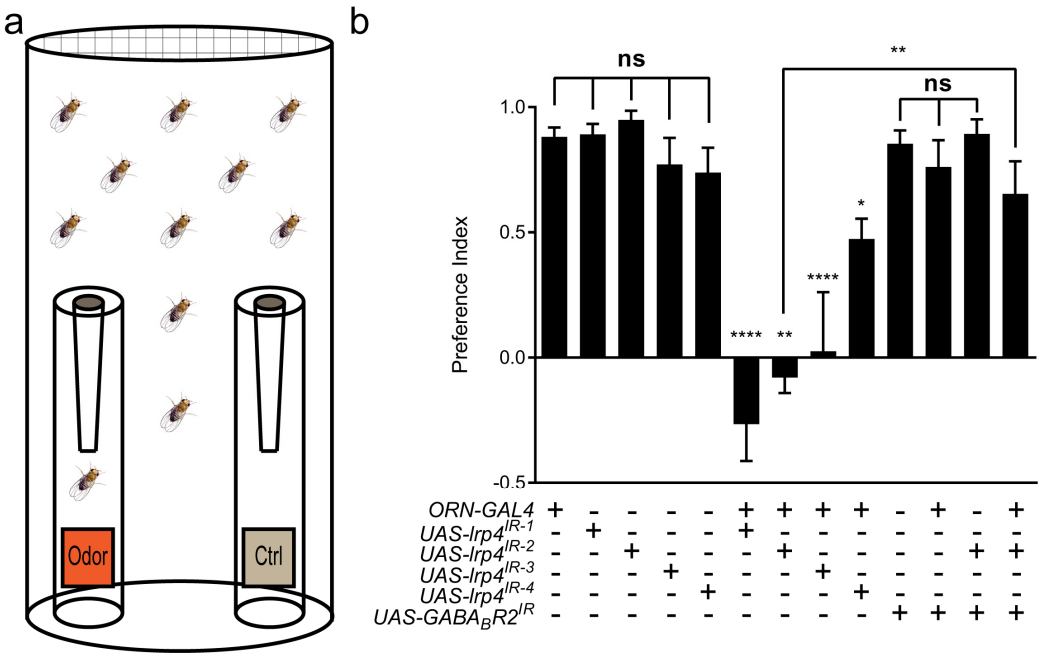

Figure 6. Loss of presynaptic LRP4 abolishes olfactory attraction behavior.
(a) Cartoon of the olfactory trap.
(b) Quantification of preference index [(# of flies in odor vial – # of flies in control vial) / total # of flies] between apple cider vinegar (odor) and water (ctrl). Genotypes are indicated below. Control flies with only a *GAL4* or *UAS-RNAi* transgene demonstrate high preference for the attractive odorant in apple cider vinegar. Flies expressing *Irp4* RNAi in ORNs have this attraction abrogated. Flies expressing RNAi against $GABA_BR2$ in ORNs still display robust attractive behavior while concurrent expression with *Irp4* knockdown largely suppresses the loss of attractive behavior. To ensure an equivalent number of transgenes in each genotype, *UAS-mCD8-GFP* was included (not listed) to control for potential transgenic dilution.
****, $p < 0.0001$; **, $p < 0.01$; *, $p < 0.05$; ns, not significant. Statistical comparisons (one-way ANOVA with correction for multiple comparisons) are with control unless otherwise noted.

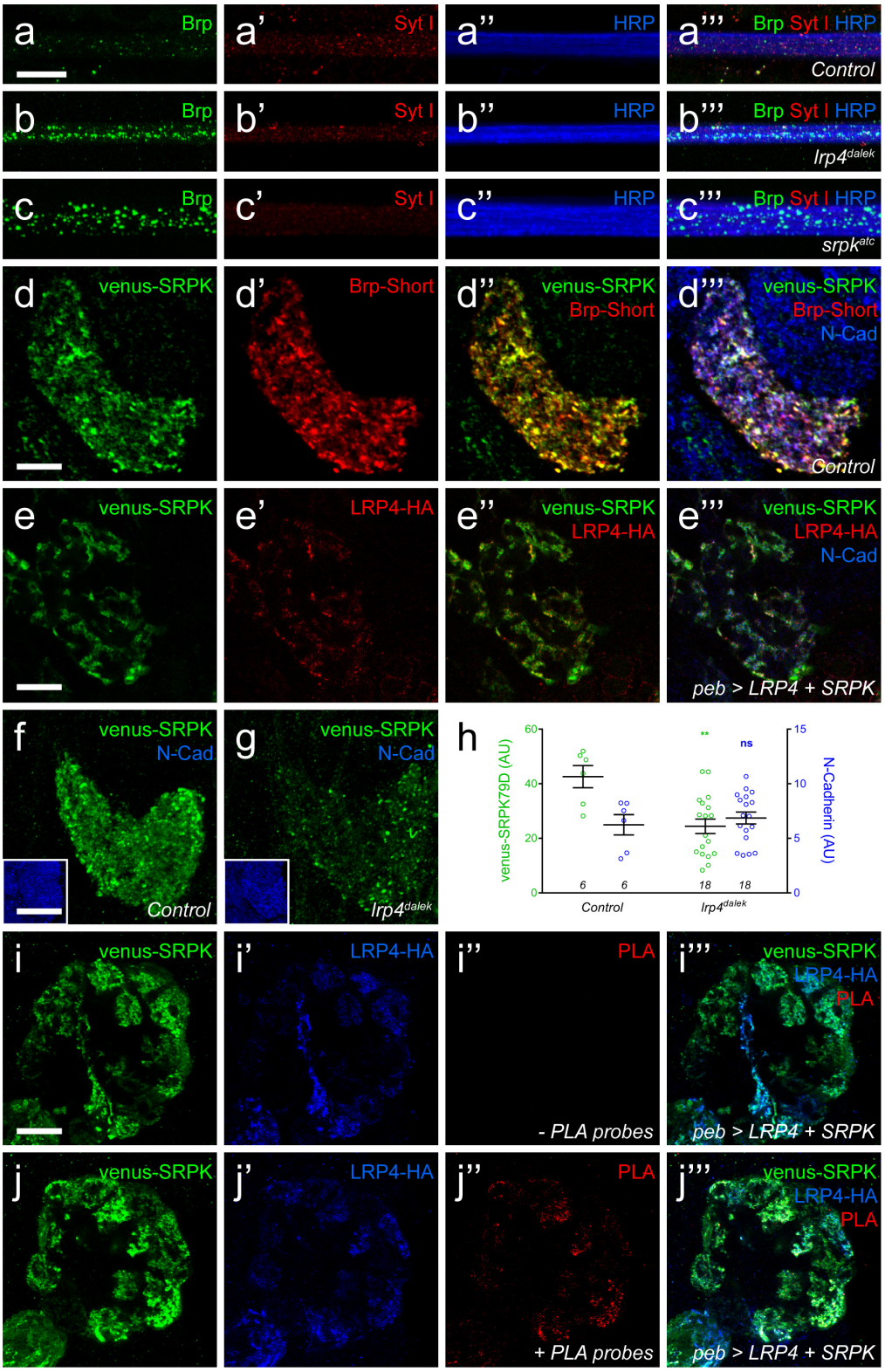

Figure 7. LRP4 is required for normal synaptic SRPK79D localization in the CNS. (a-c) Representative images of larval transverse nerves stained with antibodies to Bruchpilot (Brp, green), Synaptotagmin I (Syt I, blue), and HRP (red). Loss of *lrp4* (b,

lrp4^{dalek}) and *srpk79d* (c, *srpk*^{atc}) result in improper axonal accumulations of Brp. This is not a general trafficking defect, as Syt I is absent from focal accumulations.
(d) Representative high magnification confocal slice of VA1v ORNs expressing Brp-Short-mStraw and venus-SRPK79D and stained with antibodies to mStraw (red), GFP (green), and N-Cadherin (blue). SRPK79D largely colocalized with Brp-Short-mStraw but Brp-Short-positive / SRPK79D-negative and Brp-Short-negative / SRPK79D-positive puncta were also observed (d'').
(e) Representative confocal slice within a single antennal lobe glomerulus of a brain expressing venus-SRPK79D and LRP4-HA in all ORNs, processed for proExM, and stained with antibodies to venus (green), HA (red), and N-Cadherin (blue). Distinct regions of overlap between venus-SRPK79D and LRP4-HA (e") are observed, though this represents a subset of venus-SRPK79D localization.
(f-g) Representative high magnification single confocal slices of the antennal lobe where all ORNs are expressing venus-SRPK79D and LRP4-HA via the *pebbled-GAL4* driver and the brains subsequently using proximity ligation assays to determine whether the two proteins were close enough to interact. The brains were stained with antibodies to venus (green) and HA (blue) and PLA-specific probes (red) to detect proximity ligation events. When PLA-specific probes are not added, no signal is observed (f") but when present, positive PLA signal (g") indicates close physical proximity between LRP4-HA and venus-SRPK79D. Positive PLA signal represents a subset of SRPK79D or LRP4 expression, as in (e).
(h-i) Representative high magnification confocal maximum intensity projections of VA1v ORN axon terminals expressing venus-SRPK79D in control (h) and *lrp4*^{dalek} (i) backgrounds and stained with antibodies to GFP (green) and N-Cadherin (blue, inset). Loss of *lrp4* results in reduced synaptic SRPK79D.
(j) Quantification of venus-SRPK79D (green, left axis) and N-Cadherin fluorescence (blue, right axis). SRPK79D fluorescence is markedly reduced in *lrp4*^{dalek} animals, but N-Cadherin staining is unaffected, demonstrating specificity.
**, $p < 0.01$; ns, not significant. Statistical comparisons (one-way ANOVA with correction for multiple comparisons) are with control unless otherwise noted.
Scale bars = 10 μm (a-d, h-i), 25 μm (e), 20 μm (f-g), 33 μm (h-i insets).

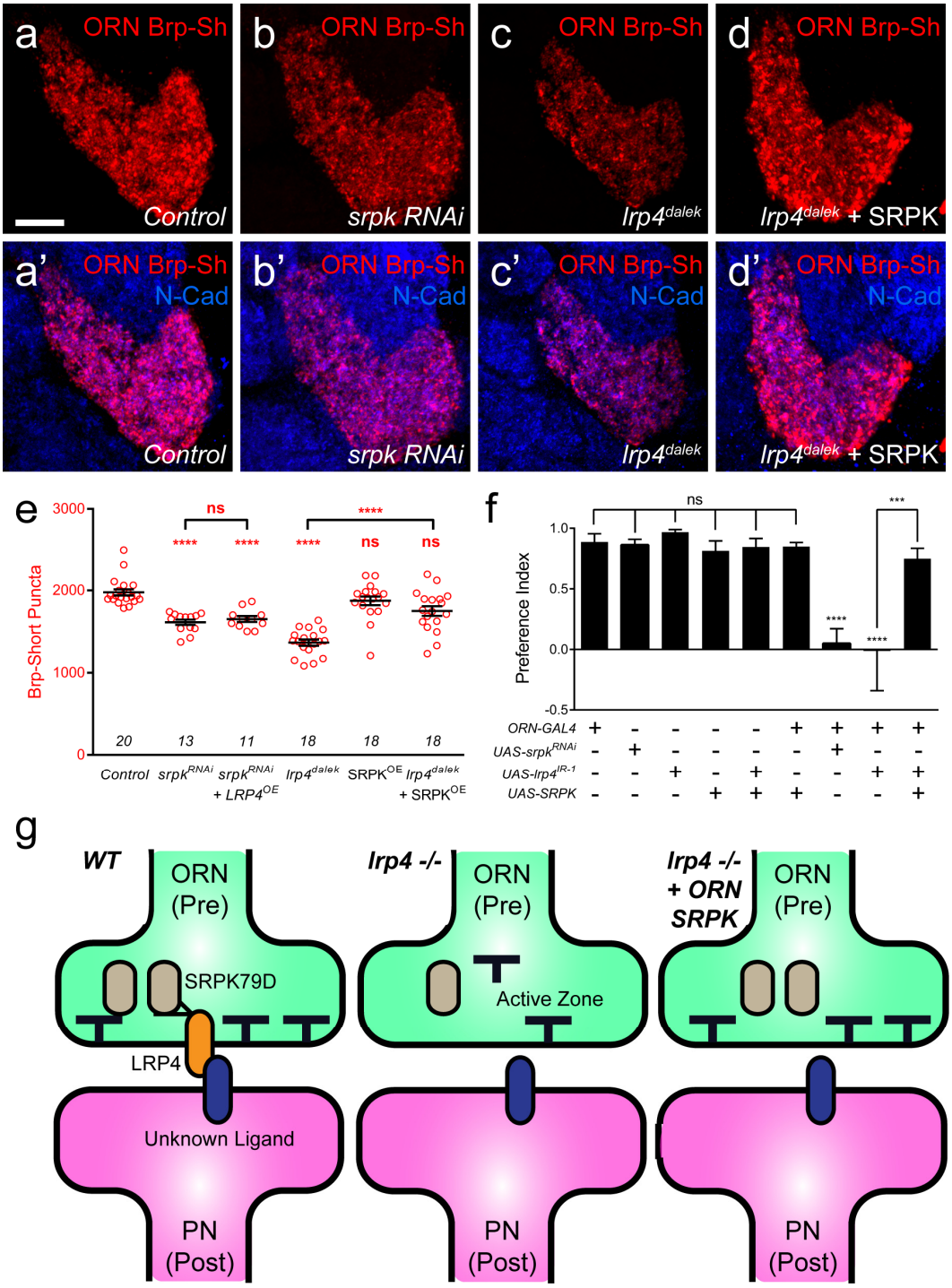

Figure 8. SRPK79D and LRP4 genetically interact to control synapse morphology and function.

(a-d) Representative high magnification confocal maximum intensity projections of VA1v ORN axon terminals in males expressing Brp-Short-mStraw and stained with antibodies to mStraw (red) and N-Cadherin (blue). Presynaptic RNAi against *srpk79D* (*srpk RNAi*) reduces the number of puncta, but less so than loss of *lrp4* (*lrp4*^{dalek}). Presynaptic

overexpression of SRPK79D in an *lrp4*^{dalek} background (*lrp4*^{dalek} + *SRPK*) restores puncta number to control levels.
(e) Quantification of Brp-Short-mStraw puncta. Note that overexpression of SRPK79D in an otherwise wild-type background has no gain-of-function effects on puncta number. Further *srpk79D* function is needed to enable the LRP4 overexpression-induced increase in synaptic puncta number.
(f) Quantification of preference index in the olfactory trap assay. Flies overexpressing SRPK79D in ORNs show strong attractive behavior, while ORNs expressing RNAi against *lrp4* or *srpk79D* abrogate attraction to apple cider vinegar. This phenotype can be suppressed by concurrent overexpression of SRPK79D. *UAS-mCD8-GFP* (not listed) was used to ensure equivalent numbers of transgenes in each genotype.
(g) A model for LRP4 function at olfactory synapses. At wild-type axon terminals, LRP4 in presynaptic ORNs (orange) interacts with a putative postsynaptic partner (blue), resulting in SRPK79D (beige) retention at the terminal and a full complement of active zones (black T). Here, the putative ligand is depicted as having a postsynaptic PN source, but alternate sources (such as glia or local interneurons) are also possible. In the absence of LRP4, less synaptic SRPK79D is present and active zone number is reduced. The size of the terminal itself does not change but the synapse number (i.e., number of active zones) within that terminal space is reduced. Further, T-bar defects like a floating T-bar can also be seen. SRPK79D overexpression in an *lrp4* mutant restores synaptic SRPK79D and active zone number, despite the absence of LRP4. Thus, the LRP4 largely functions in synaptic organization through downstream SRPK79D.
****, $p < 0.0001$; ***, $p < 0.001$; ns, not significant. Statistical comparisons (one-way ANOVA with correction for multiple comparisons) are with control unless otherwise noted. Scale bars = 10 μm.